PB-225 083/5

MEASUREMENT AND CHARACTERIZATION OF PARTICLES IN WET SCRUBBING PROCESS FOR SOx CONTROL

Walter C. McCrone Associates, Incorporated

Prepared for:

Environmental Protection Agency

July 1973

DISTRIBUTED BY:

NTIS

National Technical Information Service
U. S. DEPARTMENT OF COMMERCE
5285 Port Royal Road, Springfield Va. 22151

EPA-650/2-73-024

July 1972

ENVIRONMENTAL PROTECTION TECHNOLOGY SERIES

MEASUREMENT AND CHARACTERIZATION OF PARTICLES IN WET SCRUBBING PROCESS FOR SO_x CONTROL

Office of Research and Development
U.S. Environmental Protection Agency
Washington, D.C. 20460

BIBLIOGRAPHIC DATA SHEET	1. Report No. EPA-650/2-73-024	2.	PB 225 083/5 3.
4. Title and Subtitle Measurement and Characterization of Particles in Wet Scrubbing Process for SO_x Control			5. Report Date July 1972 6.
7. Author(s)			8. Performing Organization Rept. No. MA Proj 2001
9. Performing Organization Name and Address Walter C. McCrone Associates, Inc. 2820 South Michigan Avenue Chicago, Illinois 60616			10. Project/Task/Work Unit No. 11. Contract/Grant No. EHSD 71-25
12. Sponsoring Organization Name and Address EPA, Office of Research and Development NERC-RTP, Control Systems Laboratory Research Triangle Park, North Carolina 27711			13. Type of Report & Period Covered Final 8/15/70-7/7/72 14.

15. Supplementary Notes

16. Abstracts. The report gives results of the development of a technique for size-selective, high-capacity particulate sampling to be used in measuring and characterizing the particles in the wet-scrubbing process for SOx control. It provides information on both wet-scrubbing system process variables, and the efficiency of scrubbers to be used at the TVA test station. The sampler, existing as a manually operated bench-scale prototype, is capable not only of fractionating the particles in the desired range, but also of tolerating the process stream environment. A preliminary evaluation indicated not only that existing hardware did not meet all requirements, but that automatic sampling was more cost effective (despite higher initial costs) than manual sampling, by at least 16 percent. However, program economics resulted in the decision to design a manually operated model.

17. Key Words and Document Analysis. 17a. Descriptors

Air Pollution
Particle Size
Measurement
Sampling
Sulfur Oxides
Cost Effectiveness
Washing
Scrubbers
Wind Tunnels
Field Tests
Dust Filters
Dust
Dust Collectors
Fly Ash
Cyclone Separators
Elutriators
Flue Gases

17b. Identifiers/Open-Ended Terms

Air Pollution Control
Particulates
Characterization
Particle Collection
Cascade Impactors
Wet Scrubbing
Andersen Stack Sampler

Reproduced by
NATIONAL TECHNICAL INFORMATION SERVICE
U S Department of Commerce
Springfield VA 22151

17c. COSATI Field/Group 13B, 14A, 14B

18. Availability Statement	19. Security Class (This Report)	21. No. of Pages
Unlimited	UNCLASSIFIED	100
	20. Security Class (This Page) UNCLASSIFIED	22. Price 7.00

319040

EPA-650/2-73-024

MEASUREMENT AND CHARACTERIZATION OF PARTICLES IN WET SCRUBBING PROCESS FOR SO_x CONTROL

by

Donald A. Brooks

Walter C. McCrone Associates, Inc.
2820 South Michigan Avenue
Chicago, Illinois 60616

Contract No. EHSD 71-25
Program Element No. 1A2013

EPA Project Officer: D. Bruce Harris

Control Systems Laboratory
National Environmental Research Center
Research Triangle Park, N.C. 27711

Prepared for

OFFICE OF RESEARCH AND DEVELOPMENT
U.S. ENVIRONMENTAL PROTECTION AGENCY
WASHINGTON, D.C. 20460

July 1972

This report has been reviewed by the Environmental Protection Agency and approved for publication. Approval does not signify that the contents necessarily reflect the views and policies of the Agency, nor does mention of trade names or commercial products constitute endorsement or recommendation for use.

TABLE OF CONTENTS

		page
I.	Introduction	1
II.	Phase I	2
1.	Review of Duct Condition at the Scrubber Test Facility	2
2.	Evaluation of the Andersen Stack Sampler	9
2.1	Prediction of Particle Collection Efficiency	9
2.2	Sensitivity Analysis of the Particle Collection Efficiency of Size Selective Particle Sampler	16
2.3.	Experimental Evaluation of the Andersen Stack Sampler	20
3.	Design of a Parallel Cyclone Size Selective Sampler	26
3.1.	Conceptual Design of the Sampler and Train	26
3.2.	Operation of Sampler	31
3.3.	Uses of Data from Size Selective Mass Sampler	32
3.4.	Introduction to Cyclone Design	36
3.5.	Theory of Cyclone Optimization	45
3.6.	Experimental Evaluation of a Sampling Cyclone	53
4.	Review of Laboratory Equipment	57
4.1.	Wind Tunnel and Lab Prep	58
4.2.	IIMC Evaluation	64
5.	Field Test: Kansas Power and Light Company	65
5.1.	Background	65
5.2.	Experimental Plan	65
5.3.	Description of KPL Tests	66
5.3.1.	Time Priorities	66
5.3.2.	Completed Tests	66
5.4.	Series Cyclone Efficiency	70
5.5.	Probe Deposition	70
6.	Field Test: Shawnee Power Plant	71
7.	Deposition of Particles in a Horizontal Sampling Tube	76
8.	Prediction of Sample Bias Due to Non-Isokenetic Aspiration	82
9.	Evaluation of Filters for Parallel Cyclone Samplers	86
III.	Summary of Phase II	89
	References	91

FIGURES

No.		page
1	Particle Size Distribution at the Wet Scrubber Inlet	8
2	Particle Collection Efficiency of the Andersen Stack Sampler, Flow Rate = 0.25 cfm	12
3	Particle Collection Efficiency of the Andersen Stack Sampler, Flow Rate = 0.5 cfm	13
4	Particle Collection Efficiency of the Andersen Stack Sampler, Flow Rate = 0.75 cfm	14
5	Particle Collection Efficiency of the Andersen Stack Sampler, Flow Rate = 1.0 cfm	15
6	Comparison Size Distribution Obtained from Three Andersen Impactor Samples and a Microscopically Sized Filter Sample at KPL	21
7	Particle Deposits on Stage 6 of the Andersen Impactor	24
8	Deposition in and Around Jets on Stage 4	24
9	Layout of Size Selective Gravimetric Sampler	27
10	Components of Size Selective Sample Showing One of the Seven Flow Streams	28
11	Top View of Cyclone Set Showing Tangential Outline on Cyclone T-3A	30
12	Hypothetical Particle Size Distribution and Collection Efficiency Curve for a Wet Scrubber	33
13	Schematic Drawing of a Cyclone Showing Relevant Dimensions and Velocities	37
14	A Comparison of the Ideal and Actual Collection Efficiency	39
15	The Relationship Between a, A, and b/r_3 from the Measurements of Muschelknautz and Brumer	44
16	Dependence of the Wall Friction Coefficient λ on the Re-Number and the Relative Wall Roughness k_s/r_3	49
17	Pressure Loss Coefficients of Sharp-Edged Outlet Pipes as a Function of the Relative Inner Peripheral Velocities and the Re-Number According to Measurements	51

Figures (Continued)

No.		page
18	Overall View of the Wind-Tunnel Test Facility	58
19	Modified Auto Transmission Installed on the Wind Tunnel	59
20	Climet Light-Scattering Particle Counter with the New Photomultiplier Power Supply and a Digital Volt Meter for Setting Precise Discriminator Levels	63
21	The Pilot Scrubber	72
22	Size Distribution of TVA Samples Collected with Small Cyclone	75
23	Schematic Arrangement of Equipment for Particle Deposition Study	78
24	Arrangement of Equipment to Clean Particles Deposited in the Sampling Tube	79
25	Deposition of Particles in Horizontal Sampling Tube as a Function of Particle Size and Sampling Conditions	81
26	Comparison of Predicted Nozzle Bias with the Same Sampling Time and Nozzle Cross Section	83
27	Predicted Range of Nozzle Bias for 5-μm Particles Sampled with 1/8 in. Nozzle at Various Given Velocity Ratios at 90% Confidence Level	84
28	Predicted Range of Nozzle Bias for 5-μm Particles Sampled with 1-in. Nozzle at Various Given Velocity Ratios at 90% Confidence Level	85
29	Pressure Drop Vs. Flow Rate for Several Filters in Typical Filter Holders with Teflon Backup Filter to Reduce the Pressure Drop	88

TABLES

No.		page
1	Compositions of Flue Gas in Scrubber Inlets and Outlets, Based on 0% Excess Limestone Injection	3
2	Compositions of Flue Gas in Scrubber Inlets and Outlets Based on 0% Excess Dolomite Injection	4
3	Composition of Flue Gas in Scrubber Inlets and Outlets Based on 150% Excess Limestone Injection	5
4	Compositions of Flue Gas in Scrubber Inlets and Outlets, Based on 150% Excess Dolomite Injection	6
5	Ranges of Stream Gas Variables in the Wet Scrubber Inlets and Outlets	7
6	Particle Size Distribution at the Wet Scrubber Inlet	7
7	Particle Size Collected with 50% Efficiency by Each Stage of the Andersen Stack Sampler at Four Different Flow Rates	10
8	Changes of Air Velocity and Viscosity Due to a Temperature Variation of 100°F	19
9	Summary of Andersen Sampler Data from Kansas Power and Light Company Field Test	22
10	ERC Andersen Stack Sampler Tests--2μm Mono-Disperse Aerosol (Fluorometric Analysis of Collected Dye)	25
11A	Particulate Sampling Equipment and Cost Summary	29
11B	Dimensions and Geometry of a Small Cyclone Based on U.S. P.H.S. Design	43
12	The Computer Printout for the Optimization Calculations for Cyclone T-2A	54
13	Cyclone Dimensions	55
14	Parameters for Cyclone T-1A with Q = 1 cfm	55
15	Amount of Water Required to Maintain a Given Humidity in the Wind Tunnel	60

I. Introduction

This final report is submitted in fulfillment of our contractual agreement under EHSD 71-25, modification 3. The estimated period of performance for the Scope of Work under this contract was originally August 15, 1970 through August 15, 1971. However, mod 3 resolved some previous mutual misunderstandings by extending the contract period to July 7, 1972. This amendment,(3), also deleted the request for submission of a final report and required that only a draft final report be submitted. Although this report has been submitted as a draft final report, we consider it of printable form and quality.

II. Phase I

1. Review of Duct Condition

Since the main purpose of this project is to develop a size selective particulate sampler for measuring and characterizing the particles in the wet scrubbing process for SO_x control, an understanding of duct conditions is necessary before the sampler is actually designed. The sampler should not only be capable to fractionate the particles in the desired range, but also be able to tolerate the physical conditions—such as temperature, pressure, etc., imposed by the gas being sampled.

The wet scrubbing process for SO_x removal consists of two steps—the injection of pulverized limestone or dolomite into the furnace and the scrubbing of the flue gas to remove SO_2 and particulate samples. The composition of flue gas in the scrubber inlet, therefore, would depend on the quantity and type of alkali injected into the furnace and that in the outlet would depend on the particle removal efficiency of the scrubber. Thus, our first step in this project is to obtain information on the process variables of wet scrubbing and the efficiency of the scrubbers which will be installed in the TVA test station.

With regard to process variables, Bechtel's Phase I and Phase II Reports[1,2] provide a good information source. Our study of the reports, however, revealed a lack of some data necessary for the definition of sampling interfacing.

Hoping to elicit this information, we developed individual sets of questions for Bechtel, the TVA and scrubber manufacturers and,through the assistance of our project officer, we received much of the information we requested from Bechtel and the TVA. In regard to questions posed on the scrubbers, the data is very limited since most of the scrubber manufacturers were unable to answer our questions either due to their lack of information or unwillingness to disclose proprietary information. Based on the information presented in Bechtel's Report and what we collected, the flue gas compositions are listed in Tables 1 through 4. The ranges of several important stream gas variables which effect sample designs were also computed and are listed in Table 5.

Table 1 Compositions of flue gas in scrubber inlets and outlets, based on 0% excess limestone injection. (Extracted from Process Flow Diagram M-101, with totals corrected.)

Component	mw	Inlet		Outlet	
		mph	lb/hr	mph	lb/hr
SO_2	64.06	7.6	487	0.8	49
CO_2	44.01	411.8	18,121	411.1	18,091
N_2	28.02	2,314.7	64,858	2,314.7	64,858
A	39.95	28.4	1,135	28.4	1,135
O_2	32.00	142.4	4,555	140.6	4,500
H_2O	18.02	258.9	4,665	543.5	9,791
CaO(s)	56.08	7.6	426	0.1	4
$CaSO_4$(s)	136.15	2.0	265	0.0	3
Flyash	—	**	735	**	7
Inerts	—	**	50	**	1
TOTAL	—	3,173.4	95,297	3,439.2	98,439

** not included in totals

Table 2 Compositions of flue gas in scrubber inlets and outlets based on 0% excess dolomite injection. (extracted from Process Flow Diagram M-104, with totals corrected.)

Component	mw	Inlet		Outlet	
		mph	lb/hr	mph	lb/hr
SO_2	64.06	7.6	487	0.8	49
CO_2	44.01	411.8	18,121	411.4	18,106
N_2	28.02	2,314.7	64,858	2,314.7	64,858
A	39.95	28.4	1,135	28.4	1,135
O_2	32.00	142.4	4,555	140.6	4,500
H_2O	18.02	258.9	4,665	543.6	9,792
CaO(s)	56.08	3.8	213	0.0	2
$CaSO_4$(s)	136.15	1.0	133	0.0	1
MgO(s)	40.32	3.8	153	0.0	2
$MgSO_4$(s)	120.38	1.0	118	0.0	1
flyash	—	**	735	**	7
inerts	—	**	46	**	0
TOTAL		3,173.4	95,219	3,439.5	98,453

** not included in totals

Table 3 Composition of flue gas in scrubber inlets and outlets based on 150% excess limestone injection (extracted from Process Flow Diagram M-108, with totals corrected).

Component	mw	Inlet		Outlet	
		mph	lb/hr	mph	lb/hr
SO_2	64.06	7.6	487	0.8	49
CO_2	44.01	426.1	18,752	424.4	18,678
N_2	28.02	2,314.7	64,858	2,314.7	64,858
A	39.95	28.4	1,135	28.4	1,135
O_2	32.00	142.4	4,555	140.6	4,500
H_2O	18.02	258.9	4,665	543.4	9,792
CaO(s)***	56.08	21.9	1,230	0.2	12
$CaSO_4$(s)	136.15	2.0	265	0.0	3
flyash	—	**	735	**	7
inerts	—	**	126	**	1
TOTALS	—	3,202.0	96,808	3,452.5	99,035

** not included in totals

*** including $Ca(OH)_2$ as CaO

Table 4 Compositions of flue gas in scrubber inlets and outlets, based on 150% excess dolomite injection (extracted from Process Flow Diagram M-115, with totals corrected).

Component	mw	Inlet		Outlet	
		mph	lb/hr	mph	lb/hr
SO_2	64.06	7.6	487	0.8	49
CO_2	44.01	426.1	18,752	425.3	18,717
N_2	28.02	2,314.7	64,858	2,314.7	64,858
A	39.95	28.4	1,135	28.4	1,135
O_2	32.00	142.4	4,555	140.6	4,500
H_2O	18.02	258.9	4,665	544.6	9,817
CaO(s)***	56.08	10.9	614	0.1	6
$CaSO_4$(s)	136.15	1.0	133	0.0	1
MgO(s)	40.32	11.0	443	0.1	4
$MgSO_4$(s)	120.38	1.0	118	0.0	1
flyash	—	**	735	**	7
inerts	—	**	116	**	1
TOTALS	—	3,202.0	96,611	3,454.6	99,096

** not included in totals

*** including $Ca(OH)_2$ as CaO

Table 5 Ranges of stream gas variables in the wet scrubber inlets and outlets

Variables	Inlet	Outlet
Temperature (°F)	300	128 (preheated) 250 (reheated)
Pressure (psia)	14.3	13.3
Velocity (fpm)*	3,440	3,440
Particle concentration (grains/ft^3)	5 ~ 10	0.05 ~ 0.5
Air density (grains/cm^3)	0.000813	0.000812
Air viscosity (poise)	0.00023	0.00022
Relative humidity (%)	1.76	7.73 (reheated) 90.5 (preheated)
Particle size distribution	As shown in Table 6 and Figure 1	Unknown**

* calculated from

$$V = \frac{Q}{\frac{1}{4}(\pi D^2)}$$

where $Q = 30,000$ cfm

$D = 40$ m. $= LL_o/12$ ft.

** Although the actual particle size distribution in the scrubber outlet is unknown, it is reported by Bechtel that particles larger than 5 μm will not get through the scrubber.

Table 6 Particle size distribution at the wet scrubber inlet

Cumulative percent, by weight	12.5	25	37.5	50	62.5	75	87.5	100
Particle size, μm	5.3	7.2	8.8	11	13.5	17	23.5	—

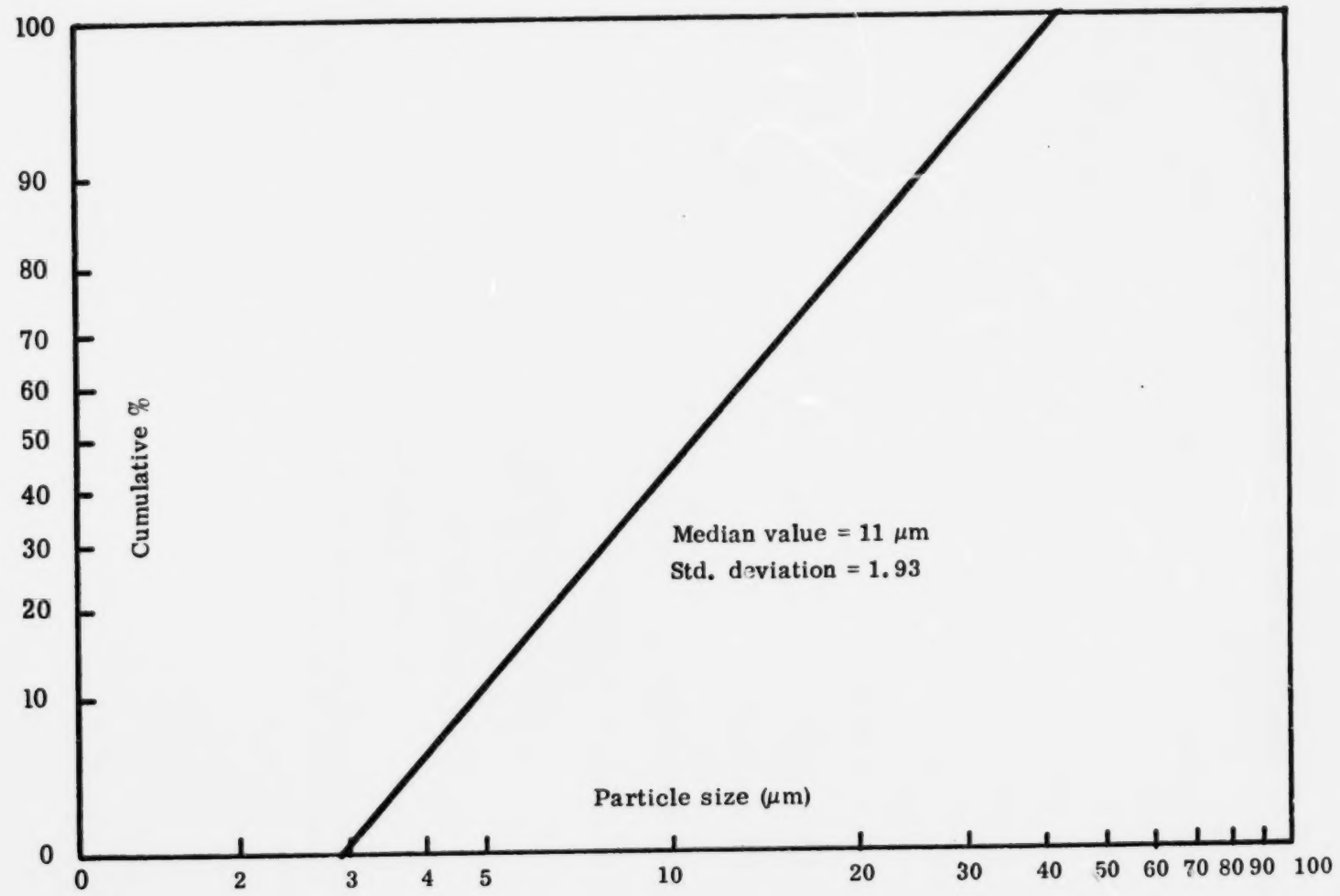

FIGURE 1 Particle size distribution at the wet scrubber inlet
(Reproduced from Figures 3-14 in Bechtel's Phase II Report)

2. Evaluation of the Andersen Stack Sampler

Since impactor stages can be used to separate particulate matter from a dust laden gas, we reviewed the feasibility of using cascade impactors as a size selective particulate device to collect particles of various size ranges both at the inlet and outlet of the wet scrubber. One of the most promising samplers of this type available off-the-shelf is the Andersen Stack Sampler. Although certain information regarding the performance of this sampler has been provided by its manufacturer and others[3,4], information on its particle collection efficiency and particle fractionation capability for various stack conditions involved in the wet scrubbing process for SO_x control is still lacking. This information is important because it predetermined the possibility of using such a device for this particular sampling job. We feel, therefore, that a performance evaluation of the Andersen Stack Sampler is desirable.

Our evaluation was performed in two parts; the theoretical prediction of the cascade impactor performance and the field test at Kansas Power and Light Company. Each of these are briefly described below.

2.1. Prediction of particle collection efficiency

The particle collection efficiency is a function of jet diameter of the cascade impactor, gas viscosity, particle density and average jet velocity. Thus, for a given duct condition, the size of the jet and flow rate determine the collection efficiency of a single impaction stage (since the flow rate determines the jet velocity).

In predicting the particle collection efficiency of the Andersen Stack Sampler, the hole sizes in each stage of the sampler were obtained from its manufacturer. Based on the size and number of holes in each plate, the jet velocity of each stage was computed for each of four different flow rates—0.25, 0.5, 0.75 and 1.0 cfm. Since these flow rates were those originally used by the manufacturer in calibrating the sampler, they were considered to be the most desirable ranges for the sampler in this project. By applying the equation describing the particle size collected with 50% efficiency[5] (X_{50}) and the equation describing the collection efficiency[5], we were able to obtain the X_{50} and collection efficiency curves at the four different

flow rates for each stage of the Andersen Stack Sampler. The results are tabulated in Table 7 and shown in Figures 2-5.

Table 7 Particle size collected with 50% efficiency by each stage of the Andersen Stack Sampler at four different flow rates

Flow rate, cfm	X_{50} of each stage, μm							
	0	1	2	3	4	5	6	7
0.25	11.0	6.9	4.7	3.2	2.1	1.1	0.7	0.5
0.50	7.8	4.9	3.3	2.3	1.5	0.8	0.5	0.3
0.75	6.3	4.0	2.7	1.9	1.2	0.6	0.4	0.3
1.00	5.5	3.4	2.3	1.6	1.0	0.5	0.3	0.2

These predictions show that, at a given flow rate, X_{50} decreases progressively as the jet diameter decreases. In contrast, for a given impaction stage, the X_{50} decreases progressively as the flow rate increases. According to the design criteria of the wet scrubber for SO_x removal presented in the Bechtel report[2], about 50% by weight of the particles in the scrubber inlet are above 11 μm, and all particles in the outlet are below 5 μm. Thus, the data detailed in Table 7 suggest that the Andersen Stack Sampler could be a good size-selective sampler at the wet scrubber outlet for any flow rate from 0.25 to 1.0 cfm. Within this range, however, the instrument will collect more than 50% of the total particulate matter sampled at the inlet on its first stage. Although it might still operate as a size-selective sampler in this case, the first five stages of the sampler would be quite overloaded in comparison with the others, and an equal eight-stage size-selective sampling could hardly be expected. This trouble can be minimized by sampling at a lower rate and by using several sampling cyclones of appropriate sizes in front of the impactor to remove the course particles.

On the basis of the theoretical prediction, it is concluded that the Andersen Stack Sampler is suitable for size-selective particle sampling both at the inlet and outlet of the wet-scrubber for SO_x control if a proper sampling flow rate is used. A flow rate of 0.75 cfm, as originally recommended by the manufacturer of the Andersen Stack Sampler, is reasonable to use.

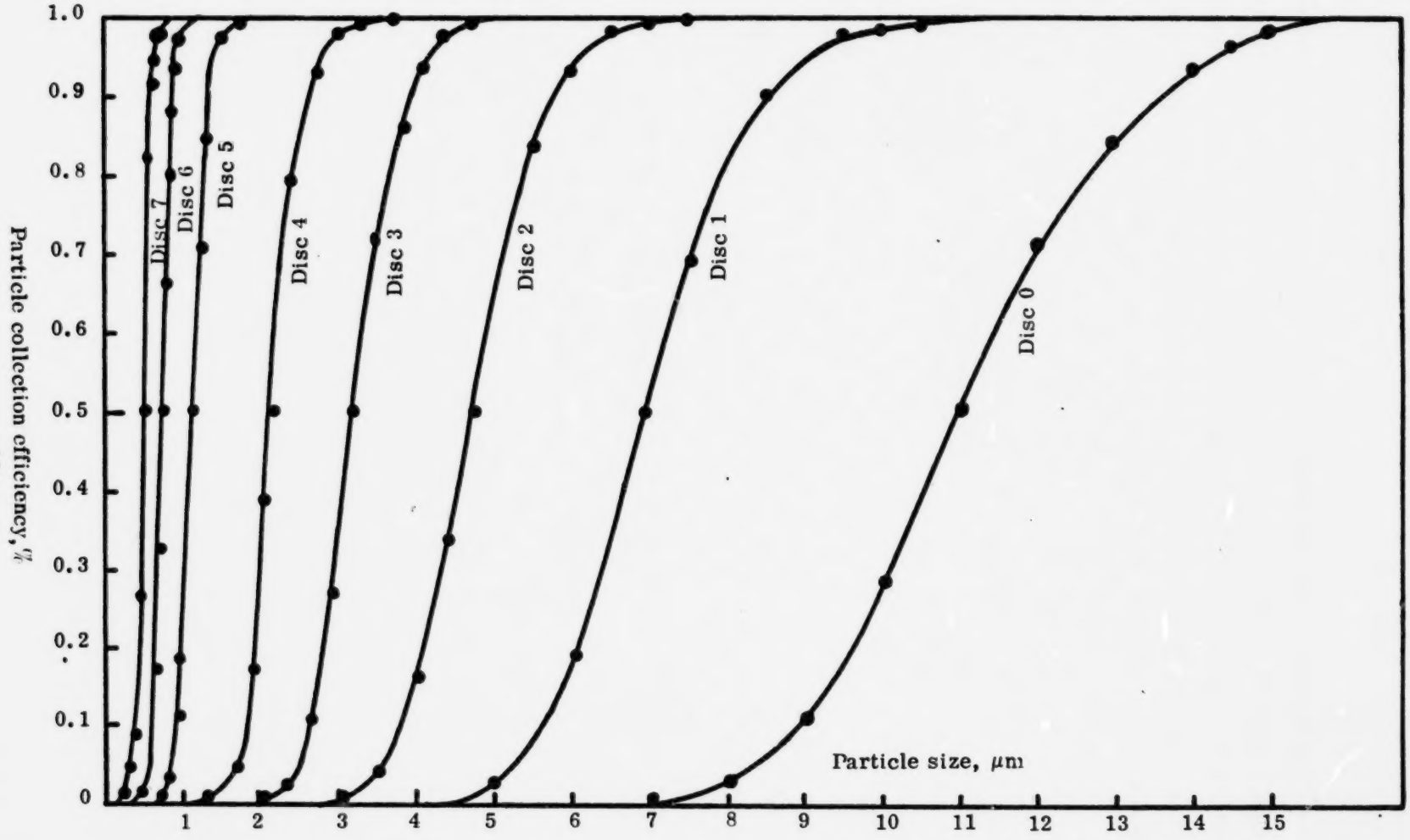

FIGURE 2 Particle collection efficiency of the Andersen Stack Sampler

Flow rate = 0.25 cfm

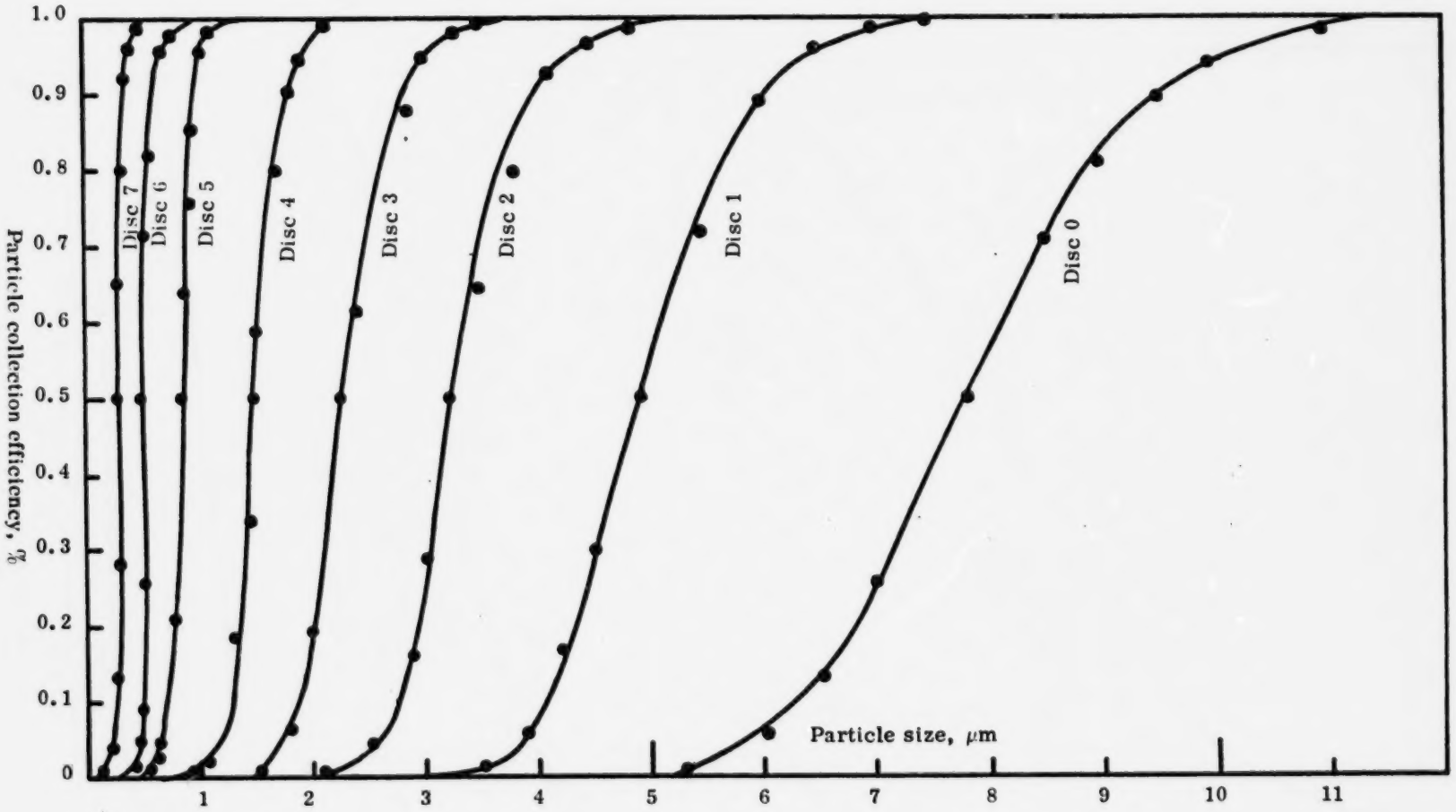

FIGURE 3 Particle collection efficiency of the Andersen Stack Sampler
Flow rate = 0.5 cfm

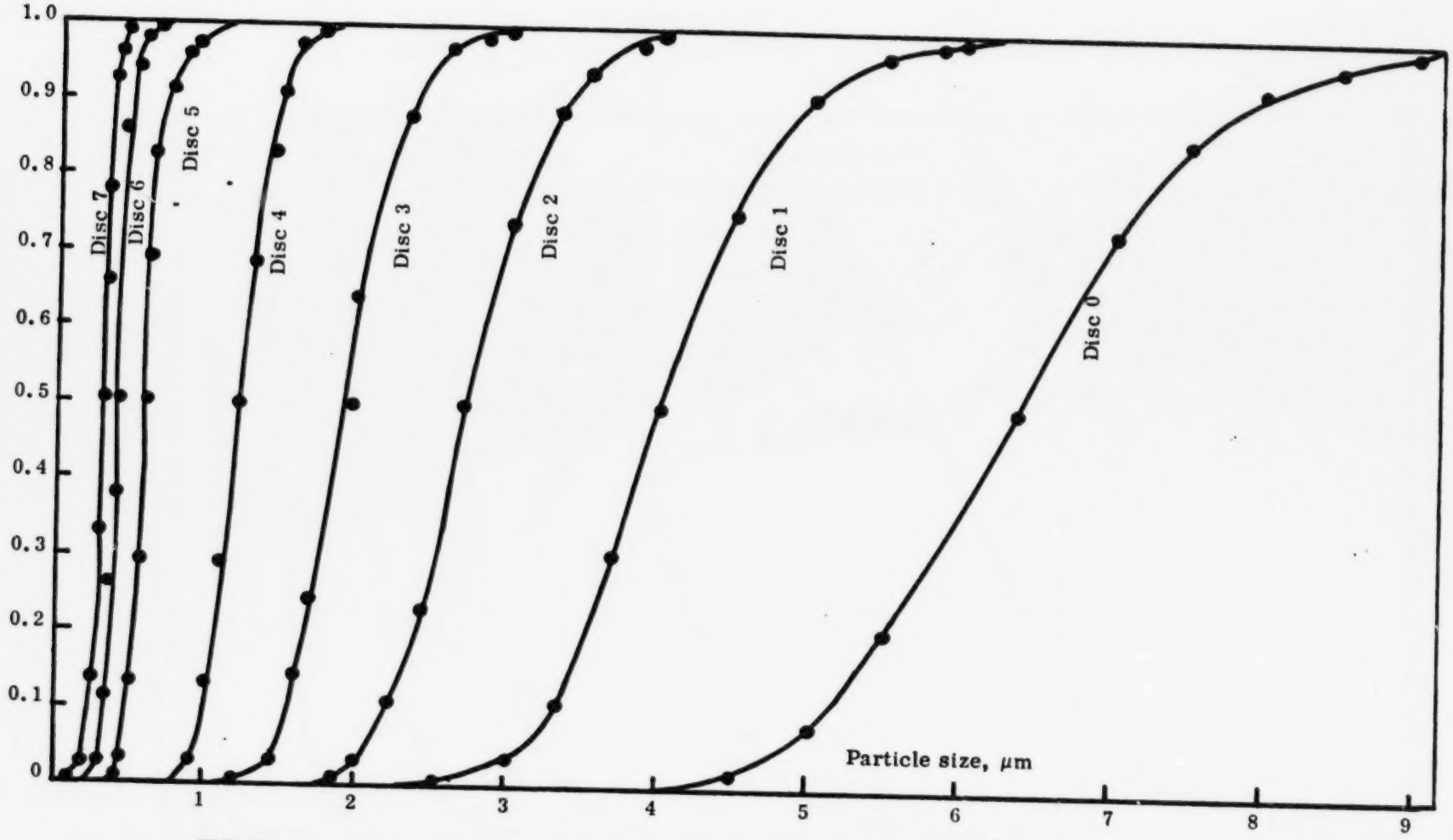

FIGURE 4 Particle collection efficiency of the Andersen Stack Sampler

Flow rate = 0.75 cfm

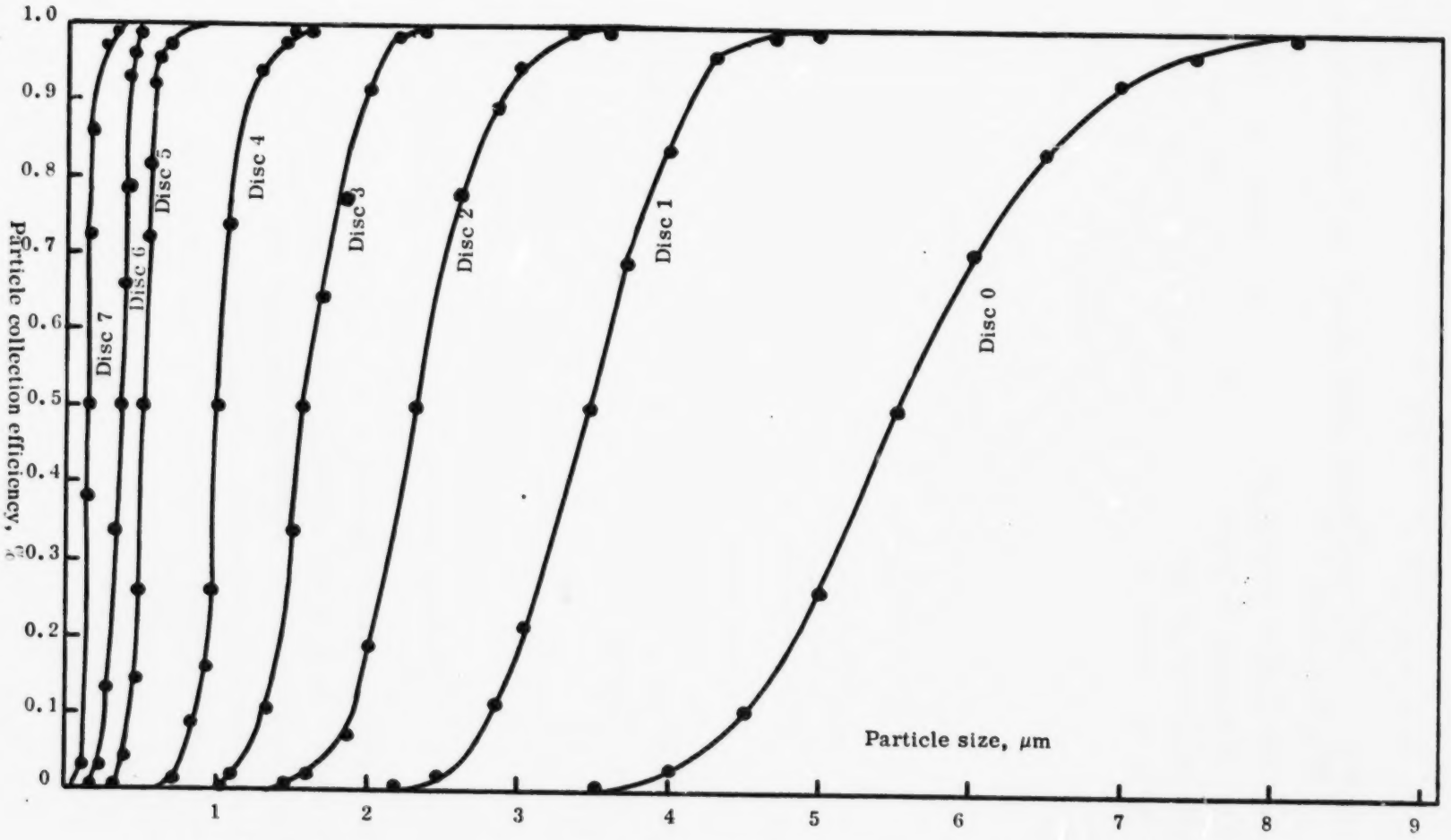

FIGURE 5 Particle collection efficiency of the Andersen Stack Sampler
Flow rate = 1.0 cfm

2.2. Sensitivity analysis of particle collection efficiency of size selective particle samplers

The particle collection efficiency of a size selective sampler, whether it is a cyclone, an impactor, or an elutriator, is dependent upon the mass flow rate, gas velocity and density, particle density and so forth. For a given sampler, the relation can be expressed as follows:

$$X_{50} = f(Q, \zeta, \mu, \rho) \qquad \text{Eq. (1)}$$

where

X_{50} = particle size collected with 50% efficiency;

Q = mass flow rate;

ζ = gas density;

μ = gas viscosity; and

ρ = particle density.

The gas density and viscosity is dependent upon gas temperature. Thus, equation (1) can be expressed as follows:

$$X_{50} = f(Q, T, \rho) \qquad \text{Eq. (2)}$$

where

T = gas temperature.

This equation indicates that in order to maintain a constant particle fractioning ability of a sampler, the flow rate, gas temperature and particle density must be kept constant. However, in actual stack or duct conditions, these three variables can vary to some extent. We therefore considered it necessary to examine sensitivity of the impactors, cyclones and elutriators to small changes in these three variables.

The analysis was made independently to examine the effects of small variations in the density of aerosol, temperature and flow rate to the variation of X_{50} or Z_{50}, and the aerodynamic particle size collected with 50% collection efficiency. An example is given here to illustrate the sensitivity of the process.

The X_{50} of the impactor can be expressed as follows

$$X_{50} = \left(\frac{2.34\, D\mu}{C \rho U_o} \right)^{0.5} \qquad \text{Eq. (3)}$$

and simplified to:

$$X_{50} = \left(\frac{BD\mu}{\rho U_o} \right)^{0.5} \qquad \text{Eq. (4)}$$

where

D = the impactor jet diameter as slit width;

U_o = the gas jet velocity;

μ = the gas jet viscosity;

ρ = the particle density; and

B = a constant of proportionality

Using equation (4) we can express the changes in X_{50} corresponding to small changes in D, μ, ρ and U_o as follows:

$$\Delta X_{50} \cong \frac{\partial X_{50}}{\partial D} \Delta D + \frac{\partial X_{50}}{\partial \mu} \Delta \mu + \frac{\partial X_{50}}{\partial \rho} \Delta \rho + \frac{\partial X_{50}}{\partial U_o} \Delta U_o$$

$$\cong \frac{1}{2} \left[\left(\frac{B\mu}{D \rho U_o} \right)^{0.5} \Delta D + \left(\frac{BD}{\mu \rho U_o} \right)^{0.5} \Delta \mu \right. \qquad \text{Eq. (5)}$$

$$\left. - \left(\frac{BD\mu}{\rho^3 U_o} \right)^{0.5} \Delta \rho - \left(\frac{BD\mu}{\rho U_o^3} \right)^{0.5} \Delta U_o \right]$$

and dividing both sides by X_{50}, we have:

$$\frac{\Delta X_{50}}{X_{50}} \cong \frac{1}{2}\left[\frac{\Delta D}{D} + \frac{\Delta \mu}{\mu} - \frac{\Delta \rho}{\rho} - \frac{\Delta U_o}{U_o}\right] \qquad \text{Eq. (6)}$$

To obtain the percent change in X_{50} we multiply this expression by 100:

$$\% \text{ change in } X_{50} \cong 50\left[\frac{\Delta D}{D} + \frac{\Delta \mu}{\mu} - \frac{\Delta \rho}{\rho} - \frac{\Delta U_o}{U_o}\right] \qquad \text{Eq. (7)}$$

Equation (4) can be rearranged to obtain Z_{50}.
This is as follows:

$$Z_{50} = X_{50}(\rho)^{0.5} \qquad \text{Eq. (8)}$$

substitutes into equation (4).
We obtain

$$Z_{50} = \left(\frac{BD\mu}{U_o}\right)^{0.5} \qquad \text{Eq. (9)}$$

and

$$\% \text{ change in } Z_{50} = 50\left[\frac{\Delta D}{D} + \frac{\Delta \mu}{\mu} - \frac{\Delta U_o}{U_o}\right] \qquad \text{Eq. (10)}$$

Equations (7) and (10) are convenient for analyzing the effects of small changes in variables.

First we will examine the effect of aerosol density variations. Assuming all other variables are constant, we have:

$$\% \text{ change in } X_{50} \cong -50\frac{\Delta \rho}{\rho} \qquad \text{Eq (11)}$$

The density of flyash particles, however, may range from 1 gm/cc to over 6 gm/cc. Since this is not a small change, equation (11) cannot be used since $\Delta\rho$ must be small enough so that the second order terms are neglible.

To determine the percent of change in X_{50} corresponding to the change in ρ from 1 gm/cc to 6 gm/cc, we use equation (4).

$$\% \text{ change in } X_{50} = 100\left[\frac{X_{50(\rho=1)} - X_{50(\rho=6)}}{X_{50(\rho=1)}}\right] \qquad \text{Eq. (12)}$$

$$= 100\left(1 - \frac{1}{\sqrt{6}}\right) = 60$$

Therefore, if ρ increases from 1 gm/cc to 6 gm/cc, X_{50} decreases 60% in comparison with its value at $\rho = 1$ gm/cc.

Now, suppose we want to examine the effect of a 100°F temperature increase relative to the collection efficiency of the sampler. We can use equation (10) by holding the slit width and the mass flow rate constant. Hence, we have:

$$\% \text{ change in } Z_{50} = 50\left[\frac{\Delta\mu}{\mu} - \frac{\Delta U_o}{U_o}\right] \qquad \text{Eq. (13)}$$

The changes of air velocity and viscosity due to a 100°F temperature increase are given in Table 8 below:

Table 8 Changes of air velocity and viscosity due to a temperature variation of 100°F

Item	Original Condition	Final Condition
Temperature (°F)	300	400
Viscosity, μ, (lb_m/ft/sec)	1.16×10^{-5}	1.75×10^{-5}
Air velocity, U_o, (ft/sec)	100	113

The percent change in Z_{50} is therefore,

$$\% \text{ change in } Z_{50} = 50\left[\frac{0.14}{1.61} - \frac{13}{100}\right] = -2.15$$

Thus, the change is about -0.02% per °F increase in temperature.

Based on the results using the technique illustrated above, it was determined, for cyclones and impactors, that if the particle density is increased from 1 gm/cc to 6 gm/cc with a constant flow rate and temperature, X_{50} decreases 60% in comparison with its value at 1 gm/cc. At constant mass flow rate, variation of temperature within ±100°F would introduce ±2% variation in Z_{50}, the aerodynamic particle size collected with 50% efficiency. For elutriators, variation of temperature within ±20°F will introduce the same percent of variation in Z_{50}. For all types of samples, precise control of the flow rate is more important than temperature control. On the basis of our analysis, the following has been concluded:

(1) Sampling cyclones, impactors and elutriators are not suitable for actual size analysis on aerosols containing a wide range of particle densities.

(2) Precise aerodynamic particle size analysis is possible and is mainly dependent upon precise mass flow rate and temperature control, with precise mass flow rate control of particular concern.

These conclusions indicate that presice flow rate and temperature control are necessary in particle sampling. Therefore, during sampling development, these ideas were seriously considered.

2.3. Experimental evaluation of the Andersen Stack Sampler

Three tests were made with the Andersen sampler during our Kansas Power and Light Company field test. The procedures used during these tests and the analysis of the results are reported in another section. The three tests were performed using sampling times of 10, 4 and 1 minute. If significant particle re-entrainment occurs as the dust builds up on the collection stages, the three indicated size distributions would differ considerably by being shifted toward smaller particle sizes with longer sampling time. For comparison purposes, a microscopically determined size distribution was also obtained from a high flow rate filter sample. The four distributions are shown in Figure 6, but their comparison is complicated by another factor besides re-entrainment. The calculated grain loadings from the three Andersen sampler tests indicate that dust concentrations in the stack changed considerably during the three tests. The Andersen

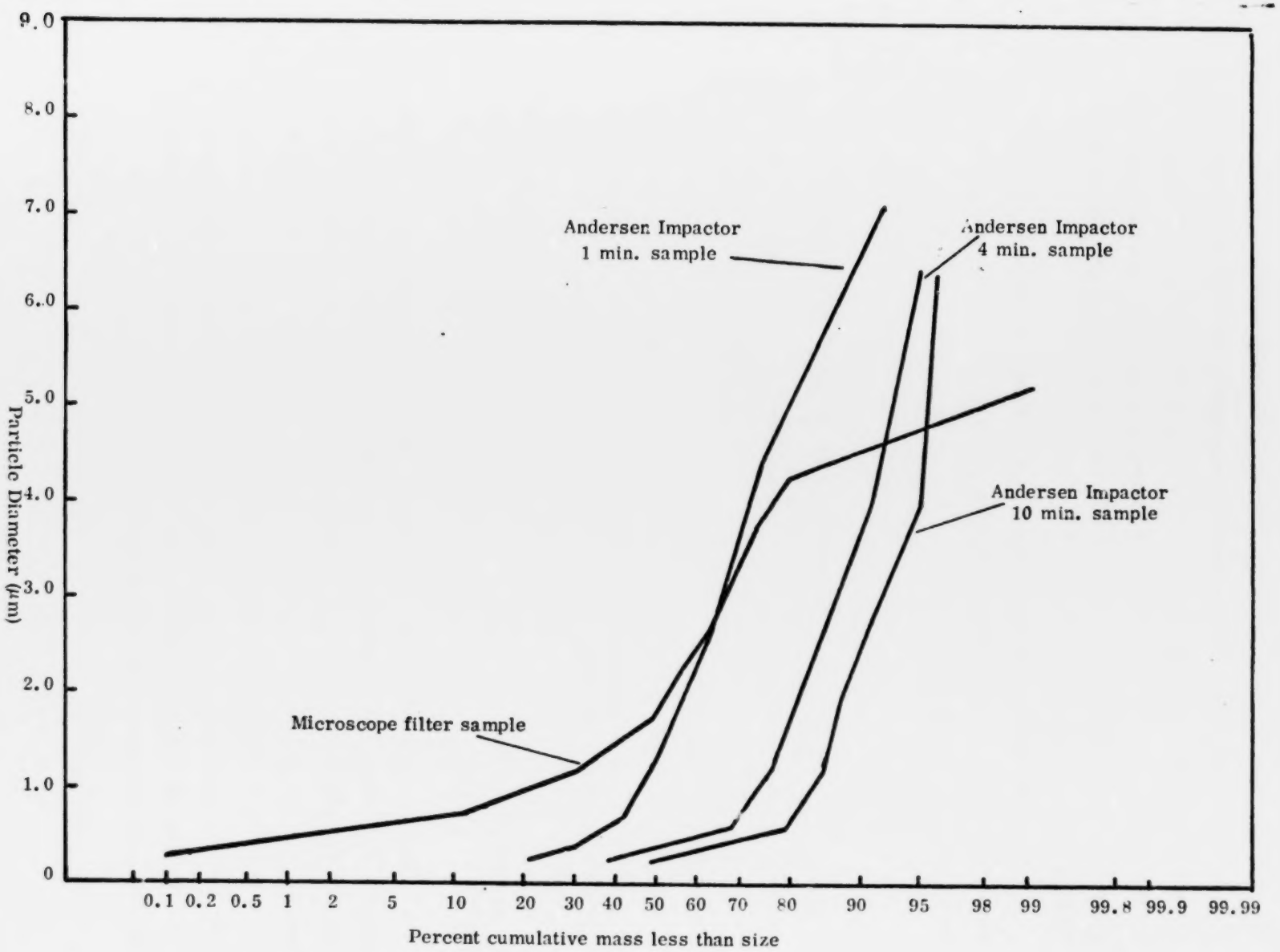

FIGURE 6 Comparison size distribution obtained from three Andersen impactor samples and a microscopically sized filter sample at KPL

sampler tests were performed with the 10 minute run first, the 1 minute run last. On the day of the testing, no soot-blowing operations were performed in the boiler since these would interfere with the emission tests being performed by York Research. By the late evening, while performing our Andersen sampler test, soot build-up in the boiler became a problem and it is likely that this led to successively higher grain loadings in the stack.

These conditions help explain the size distribution and grain loading data shown in Table 9. A much greater percentage of large particles were present during the 1 minute run.

Table 9 Summary of Andersen Sampler data from Kansas Power and Light Company field test

Item	Run 1	Run 2	Run 3
Sampling time (min)	10	4	1
Total sample weight (mg)	26.15	21.685	14.245
Flow rate through sampler (ACFM for 760°R and 22% H_2O by volume)	1.28	1.21	0.995
Grain loading (grain/ft^3 at stack conditions, dry)	0.0464	0.1322	0.3258

Despite these difficulties, it is possible from the data collected to infer that particle re-entrainment did occur in the Andersen sampler. The difference in the shape of the distribution below 1.9 μm between the 4 min and 10 min runs indicates that re-entrainment caused an increase in the weight of the samples collected on the lower stages during the 10 min run. By comparing the impactor distributions with the microscopically determined distributions, it is obvious that the impactor data significantly overestimates the concentration of small particles. Therefore, the only plausible explanation is particle re-entrainment.

Four other difficulties were encountered in using the Andersen impactor:

(1) It was difficult to weigh the sample catch on plates having 25 g tare weight;

(2) it was very difficult to clean the collected particulate matter from the plates;

(3) visual inspection of the plates indicates that a significant amount of particulate matter was collected in and around the jet holes (see Figures 7 and 8); and

(4) from 4-8% of the total sample catch was impacted on the zero stage by the entrance nozzle to the impactor.

The Environmental Research Corporation report[6] on the evaluation of the Andersen impactor was reviewed to determine if any of their results confirmed those reported above. However, the main purpose of their evaluation was to determine the reproducibility of the results obtained from the Andersen sampler for several samples taken under identical conditions. The results with a poly-dispersed aerosol having a mass medium diameter of 0.64 μm indicate that the Andersen impactor produces reproducible results. Tests with mono-dispersed aerosols of 1-to-1 mixtures of uranine and methylene blue may indicate that particle re-entrainment occurs and that the calibration constants for the impactor are not accurate. Unfortunately, aerosols of this type have densities which vary from 15-20%, depending upon the concentration of solvent in the aerosol generator and variations in water content of the bulk materials. Although the aerosol density was not reported by ERC, the work of others[7] indicates that this aerosol has a density varying from 1.2 to 1.43. This variation is large enough to account for some of the particle re-entrainment results, but it does not account for others. For example, results shown in Table 10 indicate that significant re-entrainment of 2-μm particles from stage 5 to stage 6 occurred at 0.5 cfm flow rate. This same result could have been produced by a change in aerosol density of the magnitude indicated above. However, this does not account for the significant amount of mass collected by the filter after the impactor during the same runs. Clearly, for this type of test to be conclusive, it must be performed using aerosols of constant density and their size must be monitored during the test.

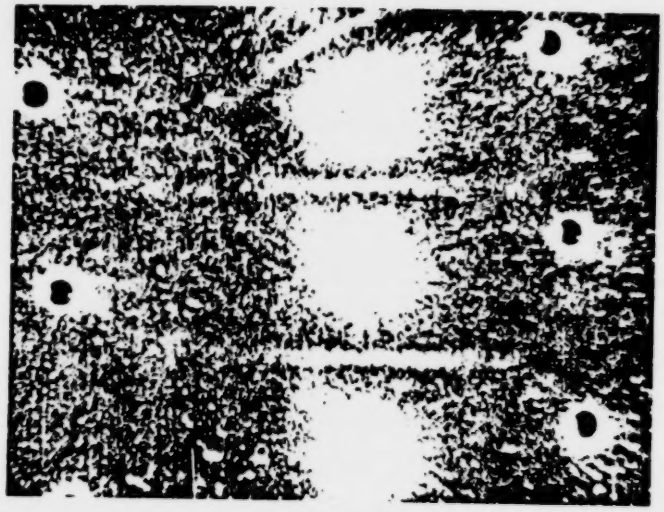

FIGURE 7

Photo shows particle deposits on stage 6 of the Andersen Impactor. Deposition around jet holes is clearly visible.

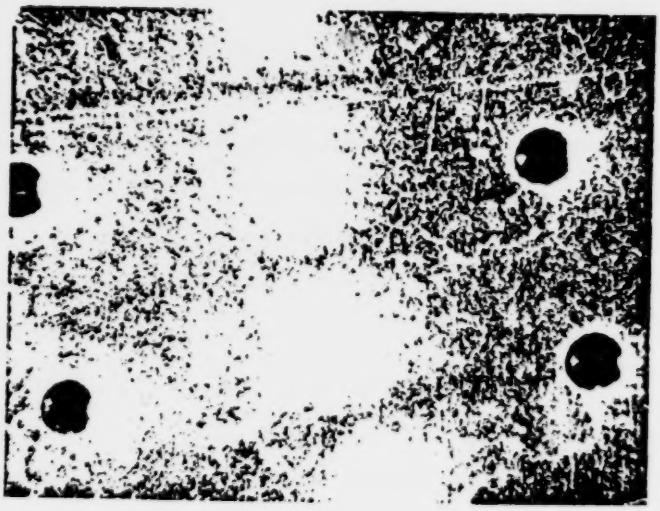

FIGURE 8

Photo shows deposition in and around jets on stage 4.

Table 10 ERC Andersen Stack Sampler Tests—2μm Mono-disperse Aerosol (fluorometric analysis of collected dye)

Stage	Percent of Total Collected Mass (1.0 cfm)		Percent of Total Collected Mass (0.5 cfm)	
	5-minute sample	15-minute sample	10-minute sample	30-minute sample
Filter	3.7	14.7	0.7	3.3
8	1.0	4.6	—	—
7	1.0	1.2	—	1.0
6	4.8	1.0	4.9	45.6
5	57.8	47.0	92.0	48.4
4	30.2	29.4	0.9	1.0
3	0.3	0.3	0.1	—
2	—	—	—	—
1	0.3	0.3	—	—
0	0.7	1.4	1.2	0.7

The failure of the Andersen impactor to perform adequately during the field test led to the consideration of other types of samplers. We concluded that an arrangement of small sampling cyclones might be feasible since cyclones are capable of collecting a large amount of sample. Our goal during the rest of this porject was then two-fold: first we had to eliminate the major sources of sampling errors in the complete sampling — for example, deposition in the transport tube, sample bias due to non-isokinetic sampling, and poor filter performance; and, secondly we had to design and evaluate a new type of cyclone sampler.

3. Design of a Parallel Cyclone Size Selective Sampler

3.1. Conceptual design of the sampler and train

A conceptual design for a parallel cyclone sampling train is shown in Figures 9 and 10; it consists of three units: (1) the sample box, (2) a control unit which contains pumps and gas metering equipment, and (3) a coolant supply system which supplies coolant for the water vapor traps for all sampling trains being used. The components used in the sampling train are listed in Table 11A.

The coolant system uses a small refrigeration unit to cool a water/glycol mixture which is being pumped through the water vapor traps and back to the refrigeration unit. This eliminates the inconvenience of using ice to cool the traps.

Particulate samples will be removed from the stack by a 3-ft x 1/2-in diameter pitobe containing a thermocouple and s-type pitot tube for measuring stack velocity and temperature. The nozzle of the probe will be designed so that a minimum of dust deposition occurs in the bend. This will be achieved in a half-inch probe by using a 4-in radius of curvature. Our dust deposition experiments indicate that a minimum deposition will occur in a 1/2-in probe when used at the flow rate planned.

When sampling at the scrubber inlet, a cyclone precollector is used to prevent large particles from entering the small cyclones, since in the small cyclones high gas velocities are obtained and could lead to the loss of the large particles by particle interaction and/or bounce. The outlet of the precollector functions as a gas manifold to divide the gas flow into seven branches. Since the gas flow in the precollector outlet is a vortex, the best aerodynamic method of dividing the flow is seven tangential outlets, as shown in Figure 11A. An inverted cone in the middle of the outlet manifold is used to maintain the vortex motion. The seven outlet flow rates are arranged so that the total flow into any quadrant of the manifold is equivalent to that of any other quadrant. For sampling at the scrubber outlet, the precollector body is replaced by an adapter which connects the probe to the outlet manifold.

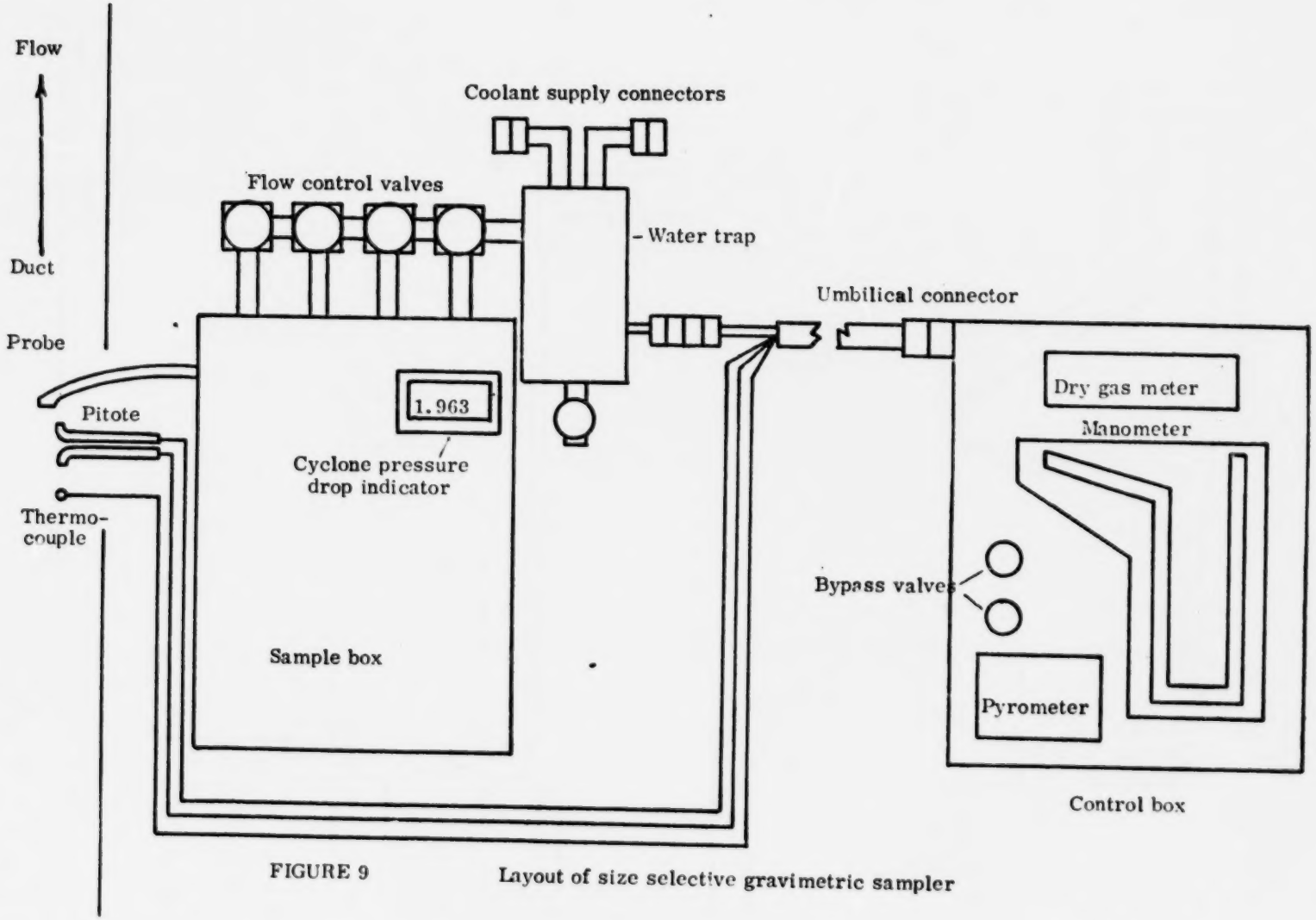

FIGURE 9 Layout of size selective gravimetric sampler

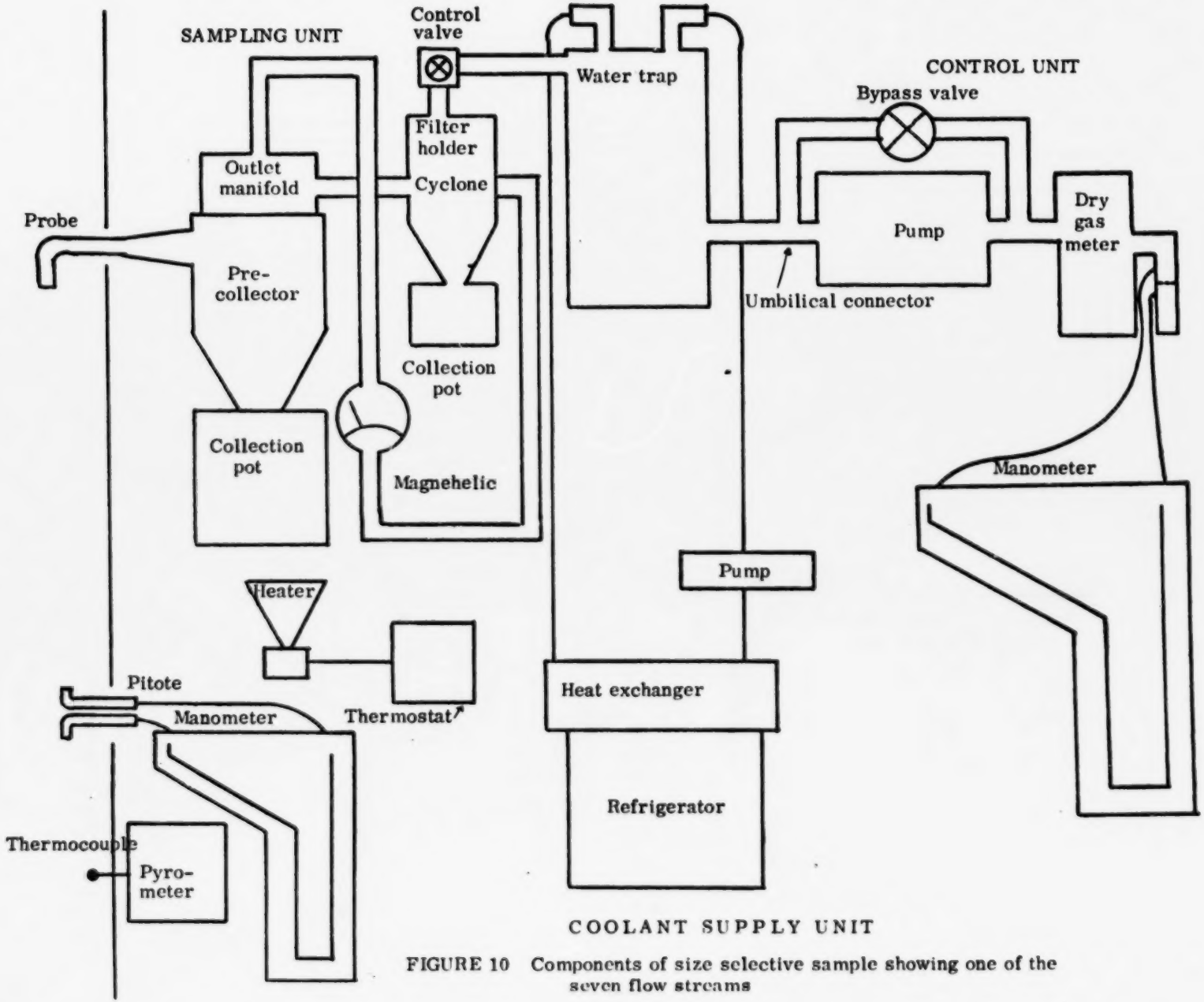

FIGURE 10 Components of size selective sample showing one of the seven flow streams

Table 11A Particulate sampling equipment and cost summary

Sampling Train Components	Quantity	Cost
Sampling probe (pitobe)	1	$ 125
Probe nozzle	1	25
Seven stage cyclone with precollector	1	3500
Gas flow valves	7	56
Gas manifold and tubing	1	100
Temperature controller and probes	2	90
Heater and blower	1	35
1/2 inch quick disconnect	4	64
Magnehilic pressure guage	6	164
Silicone o-ring	1	40
Insulated sample box	1	150
Condenser	1	150
Control Unit		
Umbilical connector	1	150
By-pass valves	4	32
Control pump (no. 0322)	1	89
Gas pump (no. 0822)	1	160
Orifice meter	1	32
Dual column manometer	1	187
Dry gas meter	1	100
Electrical switches and accessories	1	50
Toggle valve	1	5
Pipe fittings	1	50
Box	1	150
Gas meter thermometer	2	20
Pyrometer	1	45
Coolant Supply Unit		
Refrigerator, pump and heat exchanger (can be used simultaneously with all seven samplers)	1	1000
TOTAL		$6569

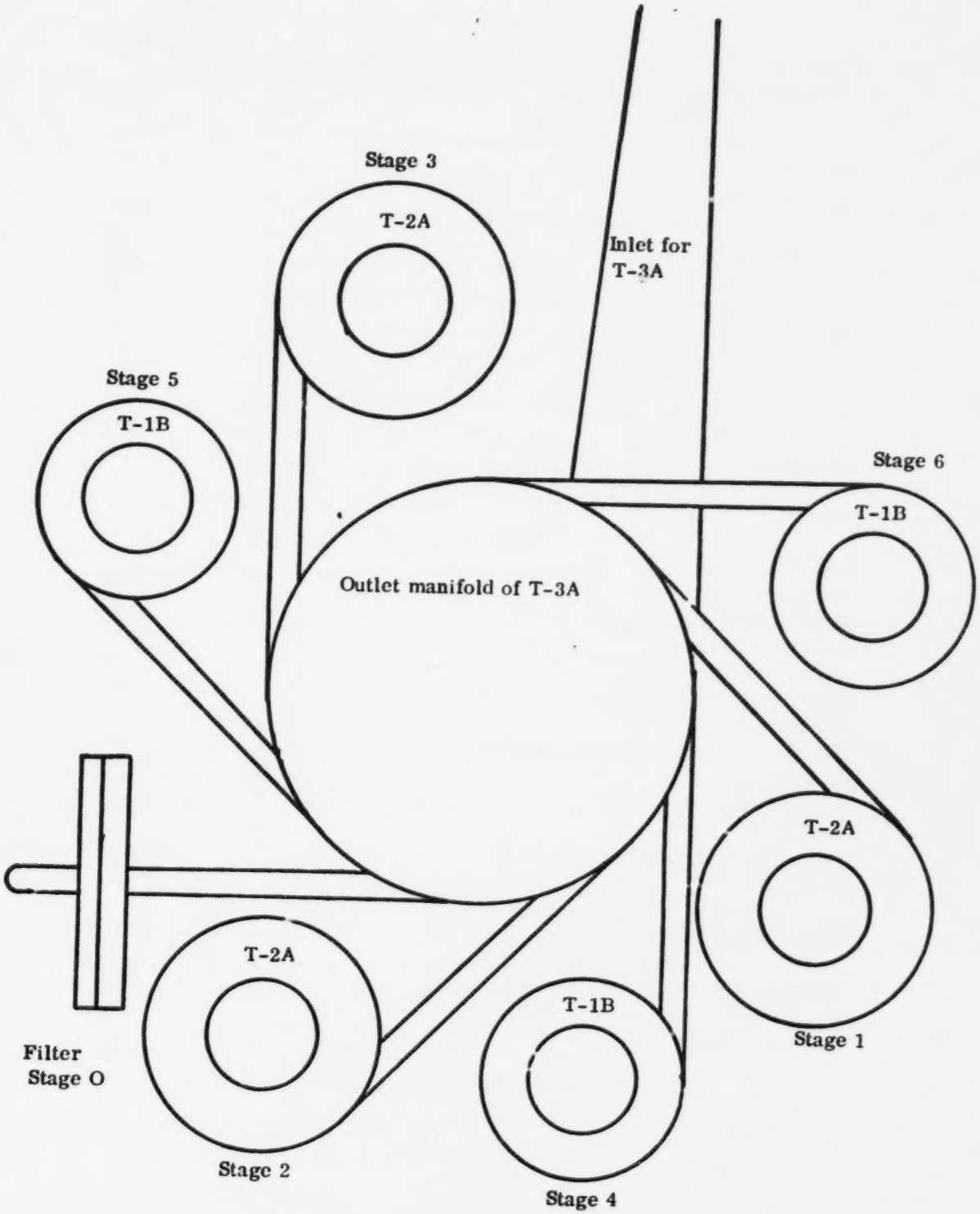

FIGURE 11 Top view of cyclone set showing tangential outline on cyclone T-3A

The seven parallel stages consist of six cyclones followed by filters and a filter stage. The pressure drop across each cyclone is indicated by magnehelic differential pressure gauges. Each cascaded cyclone-filter is made of three parts: a collection pot where collected particles are trapped, the cyclone body, and a cover plate-filter holder combination which contains the outlet pipe of the cyclone and filter. All three parts are connected by flanges with o-ring seals. This system functioned perfectly during the TVA field test. Flow control in the seven stages is maintained by valves on the exhaust side of each stage. The cyclones are maintained at 275 °F by a thermostatically controlled heater/blower in the sample box.

The control unit contains the pumps with by-pass valves, dry gas meter, pyrometer, manometers and an orifice meter. The design is similar to that used in the EPA mass train. The pump size is based on the pressure drop requirements of the filters. One pump supplies the vacuum for the six cyclones while a second smaller pump is used on the filter. Both pumps exhaust into the dry gas meter. Instantaneous flow rate measurements are made with the orifice meter/manometer. A second manometer is used to measure the velocity pressure produced by the pitot.

3.2. Operation of the sampler

Two flow conditions must be satisfied while sampling: isokinetic conditions must be maintained, and a constant cut point for the small cyclones must be maintained. The first condition can be maintained by varying the flow rate through the filter stage of the sampler from 0 to 2 cfm. This will vary the total sampler flow rate from 4 to 6 cubic feet per minute without affecting the flows through the six cyclones. Isokinetic conditions are maintained by the same method used in the EPA particle train. We have determined that the most economic and precise way of maintaining constant cut points in the cyclone is to maintain constant pressure drop across them. By adjusting the flow rate with the control valve, the operator can maintain a constant pressure drop throughout the sampling period. It is clear then that for isokinetic sampling two people will be required to perform sampling: one to maintain isokinetic conditions and one to maintain constant cut points in the size-selective sampler.

After a thirty minute sampling period has been completed, the sampler will be shut off and the parallel water vapor trap will be removed and transported to the laboratory. There the filter will be removed, dried in a desiccator, weighed and the amount of water collected in the water vapor trap measured. The filters can be used as the substrate for x-ray fluorescence analysis of the chemical constituents of the particulate matter collected to determine the size distribution of calcium moieties. If the precollector is being used, the particles collected in its collection pot will be weighed. To determine the total mass collected, the filter sample from stage 0 and the precollector catch, if there is one, can be used. To determine the size distribution, a mathemetical procedure[8] can be used to convert the filter weights to a size distribution.

3.3. Uses of data from the size selective mass sampler

As an example of how this data can be used, two hypothetical distributions are shown in Figure 12. A differential and cumulative distribution for the scrubber inlet and scrubber outlet are shown. The distribution for the inlet is an extrapolation of data obtained from a Bahco analysis of TVA flyash limestone mixtures. If we assume a scrubber mass collection efficiency of 98% and the outlet particle size distribution as shown, it is possible to calculate the scrubber size efficiency curve as also shown. The calculation is:

$$E = \frac{A - B(1 - K)}{A}$$

where

A = the fraction of particulate mass in the scrubber inlet of size X;

B = the fraction of particulate mass in the scrubber outlet of size X;

K = the fractional mass removal efficiency of the scrubber; and

E = the scrubber collection efficiency of particle size X.

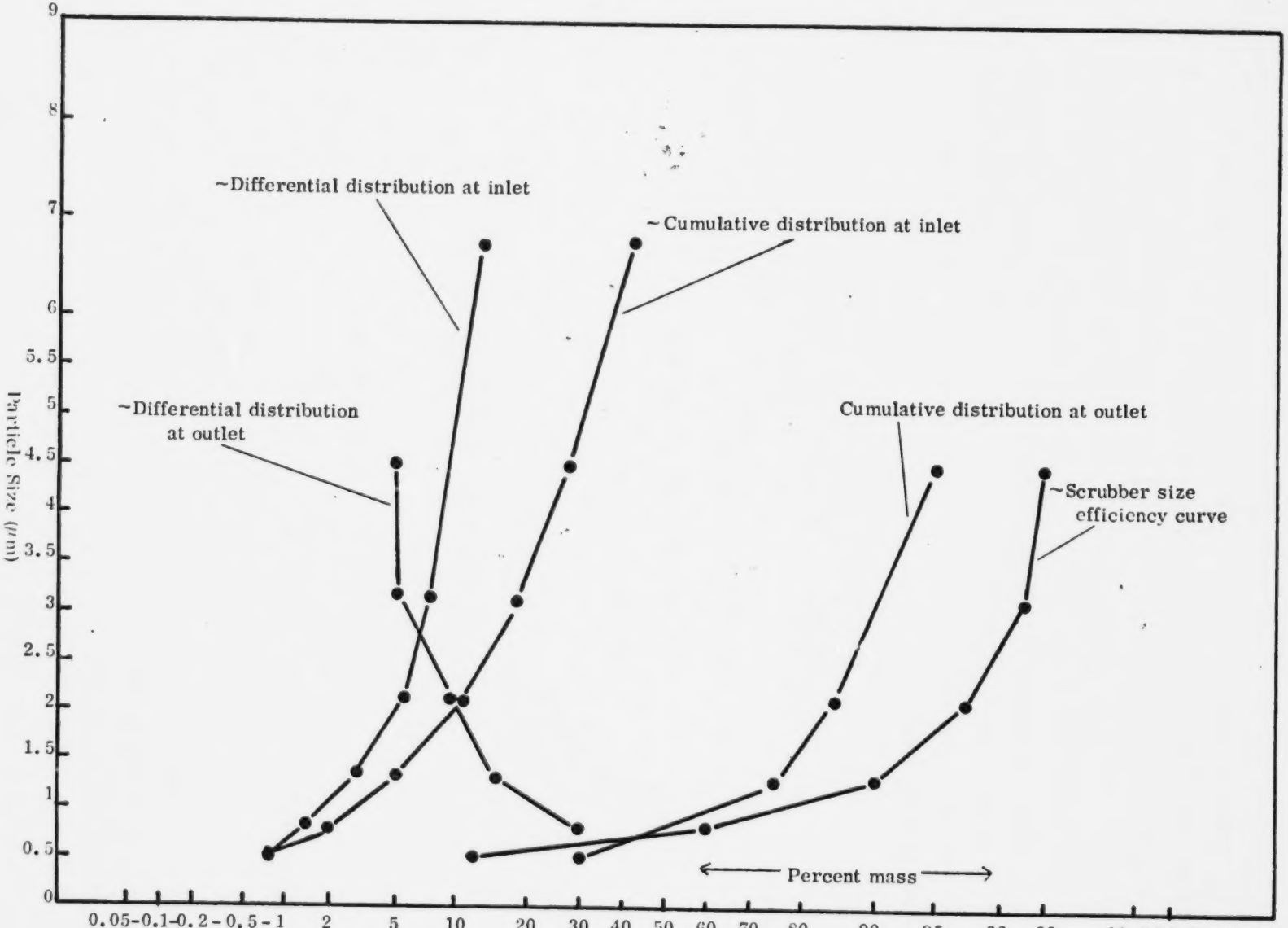

FIGURE 12 Hypothetical particle size distribution and collection effiency curve for a wet scrubber

There is actually another way of handling the particle size data which is simpler and more accurate. All particle collectors—whether scrubbers, cyclones or lungs—select particles based on the particle settling velocity and not its diameter. It is possible to calculate particle diameters from settling velocities if the particle density ρ_s, gas density ρ_g, and gas viscosity η are known. For particles of one micrometer or smaller, an additional term — the particle slip correction factor—must be calculated which allows for particle slip. The effect of these complications is readily apparent by comparing the collection efficiency equations for cyclones when stated for settling velocity W* and particle diameter d_{50}:

$$W^* = \frac{V_r}{U_i^2/r_i g;}$$

where

V_r = the radial velocity;

U_i = the peripheral velocity; and

g = the acceleration of gravity.

$$d_{50} = \left(\frac{18\eta V_r r_i (1 + 1.23\ell/d_{50})}{U_i^2 (\rho_s - \rho_g)(1 + 3.32\ell/d_{50})} \right)^{1/2}$$

where

ℓ = the mean free path in the stack gas.

Similar equations can be written for the collection of a wet scrubber. Since the gas stream conditions and particle density will be different for the inlet and outlet streams, it will be necessary to measure these parameters while sampling if particle size data is used for scrubber efficiency determinations. It would be difficult and expensive to obtain experimental values for the slip correction factor although estimates can be calculated. Since cyclones are settling velocity selectors, the particle size data obtained with them would contain fewer uncertainties if it were used in the form of particle settling velocities instead of particle diameters.

The isokinetic experiments to improve the accuracy of our theoretical model will be performed during Phase A of our work plan. We will use the light scattering particle counter to sample, size and count particles in wind tunnel tests. Such a test can be performed in approximately 160 man hours.

Manpower requirements

According to Bechtel's data, a typical test with the scrubbers will require 8 hours. Sampling may begin as soon as steady state conditions are reached. Preparations for sampling include cleaning and assembling equipment and loading preweighed filters into the sampler. This will require about one man hour per sample and the task can be performed by either sampling personnel or a lab technician. Transporting the sampling unit to the sampling point and allowing the cyclones to reach operating temperature requires about 15-30 minutes. After a sample has been collected, the reverse of the above steps is required with about the same time requirements. The only difference is that cleaning the equipment is unnecessary. A total of about 3 man hours per sample will be required before and after sampling and the lab analyses will require one man hour per sampling.

Summary of Manpower Requirements

Operation	No. of Men	Total Man Hours
Sampling		
1. Clean and assemble equipment	2	1
2. Adjust equipment	2	1/4
3. Sampling	2	1
4. Filter removal and transport to lab	1	1/2
		2-3/4
Laboratory Analysis		
1. Preweigh filters	1	1/4
2. Dry and reweigh filters	1	1/2
3. Calculate and report data	1	1/4
		1

3.4. Introduction to cyclone design

The major advantage of using a cyclone as a size selective sampler is its ability to collect a large sample without re-entrainment. This property is inherent in the way of cyclone functions. Gas enters the cyclone through the side by tangential inlet pipe and leaves the cyclone through an axial exit pipe. This arrangement produces a vortex in the body of the cyclone which exerts considerable centrifugal force on particles suspended in the air stream. For a particle to be collected by the cyclone, the centrifugal force acting on it must be greater than the opposing viscos forces of the gas. When this occurs, the particles accumulate at the walls where a downward secondary flow of the gas causes them to be collected at the bottom of the cyclone in a collection pot and all that is required to collect a given mass of sample is a large enough collection pot.

The prediction of cyclone performance is the greatest difficulty in the use of cyclones in a size selective sampler. The major difficulty is the inability to calculate flow conditions in a cyclone. A few methods of making these calculations after considerable simplification of the flow pattern have been developed. As a result, no sound theoretical methods are available for determination of the effects of change[3] in cyclone geometry on particle efficiency.

In one simplified theoretical approach, the centrifugal force acting on a particle in a simple vortex is calculated and set equal to the momentum of a particle falling in still air with a terminal velocity of w. Under these circumstances where the two forces acting on the particle are exactly equal, we would expect that a particle would have exactly equal probability of escaping or being collected by the cyclone. In other words, particles with this settling velocity are collected with 50% efficiency. The equation thus derived in equation 17, where v_r is the radial velocity, u_i is the peripheral velocity at i, r_2 is the radius of the exit pipe, and g is the gravitational constant (see Figure 13). By substituting Stoke's law for the settling velocity of the particle, equation 7 can be derived for particle diameter d_{50} (see equation 18), where μ is the gas viscosity, ρ_p is the particle density, ρ_g is the gas density and the last term in parenthesis in the denominator is a simplified form of the slip correction factor. As might be expected, the greatest difficulty in using these equations is the uncertainty in knowing the two velocities in the cyclone. Using the emphorical

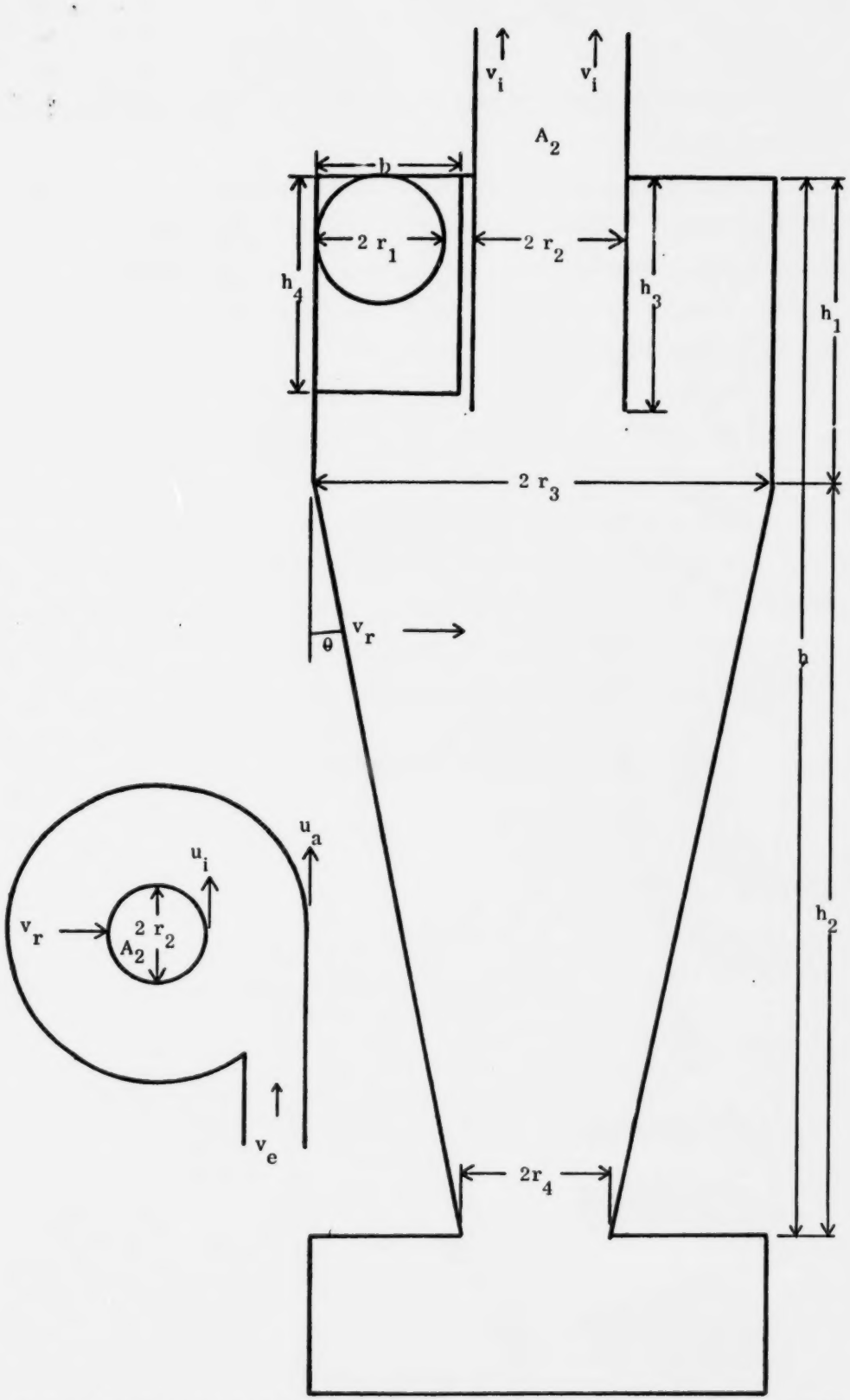

FIGURE 13 Schematic drawing of a cyclone showing relevant dimensions and velocities

data to be described later, it may be possible to use these equations with reasonable accuracy.

In an ideal cyclone all particles smaller than d_{50} would escape the cyclone while all those greater would be collected. This would lead to a vertical collection efficiency curve. Actual cyclones on the other hand have S-shaped collection efficiency curves having a straight central portion whose slope varies with cyclone geometry in an unknown way (see Figure 14).

The first task in a systematic design of a size selective sampler was to determine its operating constraints. The calculated gas viscosity, density, temperature, humidity and particle density determined in the process variable study were used for all calculations in the design of the cyclones.

The major factors affecting the number of stages used in the size selective sampler are the range of the size distribution to be sampled and the line width or size resolution of each stage. The line width of the cyclone is the experimental uncertainty in knowing exactly the collection efficiency curve for the cyclone.

Cyclone Design Equations

$$W^* = \frac{V_r}{U_i^2/r_2 g} \qquad \text{Eq. (17)}$$

$$d_{50} = \sqrt{\frac{18UV_r r_2}{U_i^2(\rho_p - \rho_8)(1 + K\ell/d_{50})}} \qquad \text{Eq. (18)}$$

$$\sigma_F^2 = \left(\frac{\partial F(x,y)}{\partial x}\right)_y^2 \sigma_x^2 + \left(\frac{\partial F(x,y)}{\partial y}\right)_x^2 \sigma_y^2 \qquad \text{Eq. (19)}$$

$$\frac{\sigma_{d_{50}}^2}{d_{50}^2} = \frac{\sigma_\mu^2}{\mu^2} + \frac{\sigma_Q^2}{Q^2} \qquad \text{Eq. (20)}$$

$$K = 0.4043 + 0.2863\,Q \qquad \text{Eq. (21)}$$

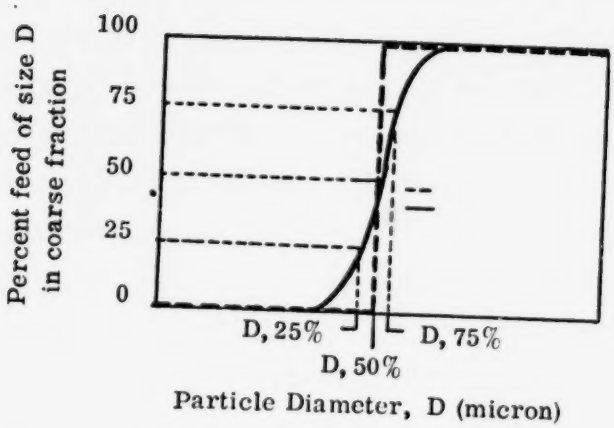

FIGURE 14 A comparison of the ideal and actual collection efficiency

At best the cut point for each stage can be one line width apart over the entire range. A more reasonable spacing, however, would be three line widths. In the case of a cyclone, two factors affect its resolution: the error in controlling the collection parameters and the error in the calibration method. The error in controlling the collection parameters of the cyclone can be estimated using the method of sensitivity analysis[9] described elsewhere.

If the performance of a system can be predicted mathematically, it is possible using this technique to determine the variability in the operation of the system using equation 19, where σ_F is the standard deviation of the function of $F(x,y)$ and standard deviations σ_x and σ_y are encountered in the parameters concerning the operation of the system. By applying this equation to the mathematical model for the prediction of d_{50}, it is possible to estimate the standard deviation of the cut-off point. By assuming that cyclone dimensions do not vary, and ignoring the variations in particle density and slip correction factor, it is possible to derive equation 20 for the standard deviation in d_{50} where the terms on the right are the fractional error in knowing the absolute gas viscosity and flow rate in the cyclone. By assuming the flow rate can be controlled to within 2-3% and the viscosity is known within 1-10% of the actual values, the variation in d_{50} will be 2.25-10.5%.

For d_{50} equal to 1 μm, the variation in collection parameters produce a standard deviation of 0.02-0.1 μm, which clearly indicates that scanning electron microscopy will be required for calibration of the collectors. By using the epidiaescope described elsewhere in conjunction with the SEM, it is possible to size particles with an accuracy equal to the resolution limit of the SEM, or ~0.025 μm. However, a large number of particles will have to be counted to obtain this accuracy and a more reasonable calibration error would be 0.1 μm. The sum of these errors, then, reduces the size of the resolution of the cyclone with d_{50} equal to 1 μm to 0.1-0.14 μm. A larger d_{50}, the size resolution will be limited by the errors in flow and viscosity measurements. For d_{50} equal to 4.5 μm, the size resolution will be about 0.14-0.49 μm. A more rigorous development of the sensitivity of the cyclone cut-off point to variations in the operating parameters indicates that the variations in wall friction may be as significant as viscosity and flow rate changes. Wall friction variations are due to the deposition of particles on the cyclone walls causing increase drag on the

rotating gas. The pressure drop across the cyclone will indicate the variations in these parameters, therefore, the most logical way of maintaining constant d_{50} is to maintain a constant pressure drop across the cyclone.

By spacing a number of cut points along the particle size distribution obtained during the Kansas Power and Light field test, we determined that a size selective sampler having seven stages and the d_{50}'s as indicated in the optimization section, would be optimum. Each stage is placed three line widths apart and the calculated percent mass and surface area of the particles collected by each stage is indicated in the table.

Again using the size distribution obtained from the KPL test and assuming a particle concentration of 0.1 grain/cfm, it was possible to calculate the necessary flow rate for each stage to collect a minimum of 10 mg during a 30-minute sampling period. The more efficient stages of the sampler must have a flow rate of at least 0.75 cfm to collect the necessary sample.

Since there will be a large population of particles greater than 5 μm in diameter at the scrubber inlet, it will be necessary to use a precollector to remove these particles. The selection of the cut point for the precollector must be made with care since a compromise must be achieved between two conflicting requirements. The large particles must be prevented from enetering the small cyclones for large particles. On the other hand, d_{50} for the precollector should not be so small that there is considerable overlap between efficiency curves of the precollector and those in some of the stages in the sampler.

Using published collection efficiency curves[10], it was possible to arrive at a reasonable compromise between the two contradictory requirements for the precollector. By setting the D_{50} for the precollector equal to D_{90} for stage 1, the overlap between the collection efficiency curve for stage 1 and the precollector will be small and the quantity of particles greater than 10 μm entering the small cyclones will be minimized. From the published data we estimated that D_{90} would be 1.5 times greater than D_{50} for stage 1 which leads to a D_{50} for the precollector of 6.75 μm. D_{90} for the precollector will be slightly larger than 10 μm.

This produced some overlap with stage 1, but the small error caused can be corrected by using the particle size information obtained by weighing the pre-collector catch.

Now that the design criteria for the sampler have been developed, it is necessary to determine the geometry and size of cyclone which meet these requirements. In order to develop as accurate a method as possible for a design of cyclones, a considerable literature search was performed. Our early attempts at cyclone design were based on the prediction equation developed by Rosin and Rammler. This includes the number of turns the gas makes in the cyclone to estimate the cut-off point of the cyclone[11]. A cyclone was designed and constructed using the geometric configuration given by the U. S. Public Health Service[12] (see Table 11B). Although no direct method exists for measuring the number of turns of the gas in a cyclone, an attempt was made to estimate it based on the pressure drop across the cyclone.

The results of the pressure drop tests on the small cyclone proved unsatisfactory as no sound relationship between the pressure drop in the cyclone and the number of turns could be developed. As a result, equations using the number of gas turns in the cyclone for predicting performance were abandoned. We also determined that the prediction model for pressure drop developed by First[13] could not be used for small cyclones since it was only possible to fit First's equation to our data for pressure drop by allowing a constant of proportionality, K, in the equation to vary with flow rate.

By fitting a least squares polynomial to the pressure drop data, we found that K varied with Q according to equation 21.

After reviewing the work of several German researchers[13,14,15,16], a design technique was developed which allowed the adjustment of all cyclone parameters and the optimization of cyclones for the collection of specific size particles.

Table 11B Dimensions and geometry of a small cyclone based on U.S.P.H.S. design (for definition of variables, see Figure 15)

$r_1 = 0.142"$

$h_3 = 6r_1 = 0.850"$

$r_3 = 4r_1 = 0.568"$

$h_1 = 16r_1 = 2.272"$

$h_2 = 16r_1 = 2.272"$

$r_2 = 2r_1 = 0.284"$

$r_4 = r_1 = 0.142"$

The optimization process consists of adjusting the various dimensions of a cyclone so that the energy losses in a cyclone are minimized while maintaining a constant cut-point. There are three advantages to be gained by using such an optimization process: first of all, no more work than necessary is expended by the cyclone air stream to remove particles of a given size. A minor result of this is smaller pump size requirements. More importantly, greater energy losses could yield increased turbulance in the cyclone and large deviations from predicted performance. We would also expect that a cyclone with minimum turbulence would have a very sharp collection efficiency curve. Lastly, the optimization design method combines all the dimensions of the cyclone together. For example, adjustments in one dimension allow more convenient construction, as appropriate adjustment of other dimensions can be made to maintain a constant cut-point.

This theoretical approach is similar to an empherical method developed by Stairmand[17] for determining the optimum geometry for a cyclone. Stairmand injected a dye into an operating, transparent cyclone and observed its vortex. By adjusting various cyclone dimensions he was able to obtain a stable vortex. The instabilities in the vortex indicate an increase in the energy loss for a given collection efficiency in the cyclone.

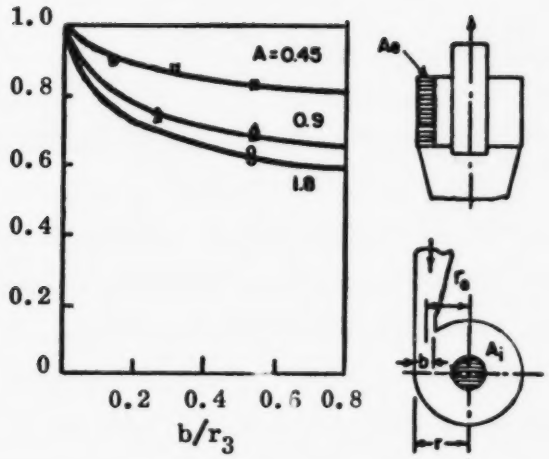

FIGURE 15 The relationship between α , A, and b/r_3 from the measurements of Muschelknautz and Brumer.

3.5. Theory of cyclone optimization

The following discussion on the theory of cyclone optimization will be limited to a rudimentary discussion of the major features. A critical review of the flow in a cyclone leading to the determination of the collection efficiency has been given by First. Extensive measurements of flows in cyclones made with a directional pitot are also reported by First.

To use the optimization process, one needs to know the basic relationships concerning flow and pressure drop in cyclones. Experimental investigations have shown that flow into the separating chamber through a tangentially attached pipe causes the jet to be constricted and therefore results in an increase in gas velocity practically without any energy loss. Mathematically, the constriction is described by

$$U_a = \frac{V_e}{\alpha'} \qquad \text{Eq. (22)}$$

Barth derived a correction factor, α, from an analysis of impulse and friction moments which relates the geometry of the inlet to the constriction,

$$\alpha = \frac{V_e \cdot r_e}{U_a \cdot r_3} \qquad \text{Eq. (23a)}$$

or

$$\alpha' = \alpha \frac{r_3}{r_e} \qquad \text{Eq. (23b)}$$

Measurements by Muschelknautz and Brumer have shown that the ratio of inlet to outlet cross sectional areas, A, effects the value of α.

$$A = \frac{a_1}{a_2} \qquad \text{Eq. (24)}$$

The values of α used in our designs are taken from the data in reference 10 for slot-shaped inlets (see Figure 15). Muschelknautz suggested that α for a circular inlet is determined using the equivalent slot width given by the length of the side of a square having the same area as the circle. However, by replacing the height and

width dimensions of a slot by the diameter of a circle, one degree of freedom is removed and α can no longer be determined independent of A. Thus, a trial and error method must be used.

To use equation 17 to determine the critical settling velocity W*, it is necessary to calculate the radial velocity, v_r, and the peripheral velocity at i, u_i. The mean value of v_r is easily calculated from

$$V_r = \frac{Q}{2\pi r_2 h_2} \qquad \text{Eq. (25)}$$

Measurements have shown that v_r departs considerably from its mean value near the bottom of the outlet pipe. This is one likely cause of the "S" shape of the collection efficiency curve.

The value of u_i can be estimated from an analysis of the moments of flow in the cyclone. The moment of momentum, M_i, required to produce a given u_i is the momentum supplied by the inlet gas, M_e, less the momentum losses, M_I, due to wall friction. By modeling a cyclone so that the friction surface is unrolled and approached by the gas as if it were a flat plate, the wall friction moment is obtained as

$$M_r = \lambda \cdot u_i u_a \cdot \pi h r_i r_a (\gamma/g). \qquad \text{Eq. (26)}$$

This serves to define the coefficient of friction, λ. From this analysis, an equation for u_i is obtained

$$\frac{u_i}{v_i} = \frac{r_3 \cdot r_e \cdot \pi}{a, \alpha + h r_e \pi \lambda} \qquad \text{Eq. (27)}$$

Introducing the dimensionless parameters

$$U_i = \frac{u_i}{V_i} \qquad \text{Eq. (28a)}$$

$$R = \frac{r_2}{r_3} \qquad \text{Eq. (28b)}$$

$$A = \frac{a_1}{a_2} \qquad \text{Eq. (28c)}$$

$$H = \frac{h}{r_3} \qquad \text{Eq. (28d)}$$

$$H_i = \frac{h_i}{r_3} \qquad \text{Eq. (28e)}$$

and substituting equation 23b into equation 27, a dimensionless equation is obtained

$$U = \frac{1}{\frac{A\alpha'}{R} + \lambda H} \qquad \text{Eq. (29)}$$

This clearly illustrates the effect of wall friction and the inlet correction factor on cyclone velocities. Until measurements by Muschelknutz proved otherwise, λ was assumed to be a constant. Frictional losses are dependent on the dust loading of the gas and the roughness and surface area of the walls. For small cyclones the frictional losses caused by the suspended dust is an order of magnitude smaller than wall friction based on experimentally verified calculations for typical dust loadings.

Muschelknautz[15] has attempted to use a Nikurodse diagram to represent the relationship between wall friction coefficients and the Reynolds number, Re, of the flow in a cyclone. The Reynolds number at the cyclone walls, Re_R, is calculated by ratioing the mass inertia and viscosity forces causing the wall friction of the flat plate representing the cyclone walls. This leads to the equation

$$Re_R = \frac{2r_e \; v_a/\nu}{2h(r_R\left[1 + (v_a/u_m)^2\right]} \qquad \text{Eq. (30)}$$

which can be transposed using the dimensionless cyclone parameters and the following relations

$$r_R = r_3\sqrt{R} \qquad \text{Eq. (31a)}$$

$$u_m = \sqrt{u_a u_i} \qquad \text{Eq. (31b)}$$

$$v_a = v_i/R(R-1) \qquad \text{Eq. (31c)}$$

to

$$Re_R = \frac{Re_i}{2H(R-1)\left[1 + \alpha' A/UR^2(R-1)^2\right]} \qquad \text{Eq. (31d)}$$

where Re_i is the Reynolds number of the outlet pipe calculated.

Based on measurements of the velocity of compressed air, oil, and water in small cyclones, the relationship between Re_R and λ is shown in Figure 16. According to these measurements, wall roughness has no affect on λ for $Re_R < 100$ and the following equation can be fitted to the data,

$$\lambda = e^{(1.1787 - 0.627 \ln Re_R)} \qquad \text{Eq. (32)}$$

During field trials with a small cyclone at TVA, we found that the pressure drop across the cyclone dropped steadily although the flow rate remained constant. A build-up of particle deposits on the walls was also observed, indicating that wall roughness may have an effect on λ even for this range of Re_R.

The total pressure loss for a cyclone consists of the losses in the separating chamber, Δp_e, and the losses in the cylinder volume below the outlet tube, Δp_i:

$$\Delta p_e = (p_a + \frac{p_2}{2} u_a^2) - (p_i + \frac{p_2}{2} u_i^2) \qquad \text{Eq. (33a)}$$

$$\Delta p_i = (p_i + \frac{p_2}{2} u_i^2) - (p_m + \frac{p_i}{2} v_i^2) \qquad \text{Eq. (33b)}$$

$$\Delta p = \Delta p_e + \Delta p_i \qquad \text{Eq. (33c)}$$

The pressure loss in the separation chamber was calculated by Barth as the difference of the speed in the intake and discharge of the assumed friction surface:

$$\Delta p_e = \frac{\gamma}{2g}\left(\frac{u_a^2 r_2}{r_3} - \frac{u_i^2 r_3}{r_2}\right) \qquad \text{Eq. (34)}$$

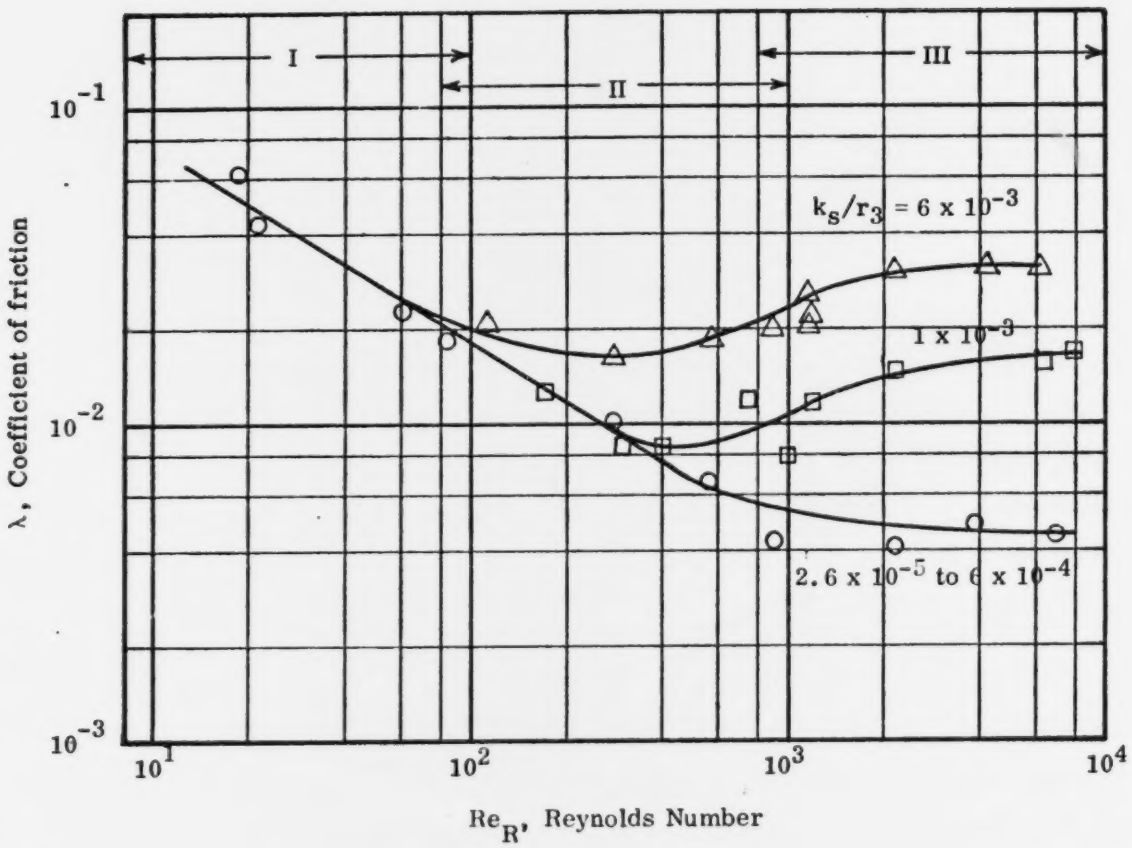

FIGURE 16 Dependence of the wall friction coefficient λ on the Reynolds number and the relative wall roughness k_s/r_3. The relative wall roughness is the ratio of particle diameter deposited on the wall to the cyclone radius.

Range I: Measurements with silicone oil M20
Range II: Measurements with water
Range III: Measurements with compressed air of 2 to 13 atm.

By defining a dimensional pressure drop coefficient as

$$\zeta_e = \frac{\Delta p_e}{\gamma \cdot v_r^2/2g} \qquad \text{Eq. (35)}$$

and substituting equations 28, 29 and 34, we get

$$\zeta_e = \frac{U^2}{R}\left[\frac{1}{(1-\lambda Hu^2)^2}\right]-1 \qquad \text{Eq. (36)}$$

The much larger loss of the outlet pipe pressure, Δp_i, and the corresponding loss coefficient ζ_i are determined from the measurements of Muschelknutz. The dependence of the loss coefficient on Re_i and U is shown in Figure 17. To allow computer assistance in the calculative procedure, a polynomial was fit to the curve for $Re_i = 2000$.

$$\zeta_i = \frac{\Delta p_i}{v_i^2/2g} \simeq 2.571 + 2.542u + 1.724u^2 \qquad \text{Eq. (37)}$$

which fits the data to within ±6%. The values of Re_i for the cyclones designed for the sampler were all close enough to 2000 to allow the use of equation 37.

Specifying the three parameters H, R, and U completely defined a cyclone since all the other variables can be derived from the above relationship if Re_i or, more properly, the flow rate, is given. Several types of cyclones having different values of the three free parameters, different size and pressure loss can be designed which will solve a particular dust removal requirement. The choice of cyclone type then must be based on size and pressure loss. To determine which cyclone from a group having equal volume has the lowest pressure loss, two parameters are introduced which serve as evaluation criteria for designing an optimum cyclone:

$$\xi^* = \frac{\Delta p}{\frac{p_g}{2} v^{*2}} \qquad \text{Eq. (38)}$$

$$B^* = \frac{u^* v^*}{2r^* g} \qquad \text{Eq. (39)}$$

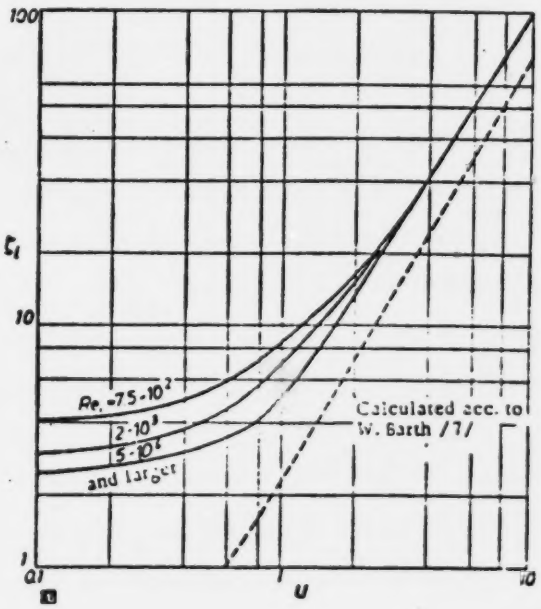

FIGURE 17 Pressure loss coefficients of sharp-edged outlet pipes as a function of the relative inner peripheral velocities and the Re number according to measurements.

The representative velocity v* is calculated from

$$v^* = \frac{Q}{\pi r^{*2}} \qquad \text{Eq. (40)}$$

where

$$r^* = (r_3^2 h)^{1/3} \qquad \text{Eq. (41)}$$

This velocity is related to the frontal face area of a cyclone of diameter r* and is proportional to the actual velocities in the cyclone. The parameter ξ^* indicates the effect of an increased pressure loss due to the result of an increased removal efficiency, as reflected by larger v*'s.

Comparing two cyclones of the same radius, (e.g., equal face area and equal gas throughput and therefore equal v*; also identical separation performances as expressed by the settling velocity, W*, of the particles collected with 50% efficiency) the respective separation index, B*, will also be identical, therefore, the unit having a lower pressure loss or ξ^* has to be considered as better. By proper substitution of the above equations, the performance can be obtained in the form:

$$\xi^* = \zeta H^{4/3} R^{8/3} \qquad \text{Eq. (42)}$$

$$B^* = \frac{1}{4 H_i H R^2 U^2} \qquad \text{Eq. (43)}$$

The optimization process consists of first estimating the wall friction coefficient, λ, and then selecting values of B*, H, R, H_i to solve equation 43 for U. Once U has been determined, ζ and A_α, can be determined. By successive iterations based on values of H and R and H_i, values of ξ^* can be scanned to find the minimum.

After the dimensionless cyclone has been designed, it is necessary to calculate the required cyclone radius to collect particles of a given settling velocity for a given flow rate, Q. The following relationship between these variables has been derived:

$$r_3 (QW^*R/2\pi g B^*)^{1/3} \qquad \text{Eq. (44)}$$

All cyclone dimensions can now be calculated. The value of Re_R calculated for the cyclone is then used to estimate a new value of λ to evaluate the original estimate. If λ is not accurate, the optimization process is repeated using the new value of λ.

Values of B* are chosen arbitraily. From inspection of equation 23 it is clear that small values of B* correspond to small values of W*. In other words, to collect small particles, a cyclone must be designed which has a small B*. Complete freedom of choice does not exist however if R is too small or λ too large for a given B*, as the cyclone inlet area approaches zero. To obtain high spinning velocity in such a cyclone the design procedure requires the inlet velocity to approach infinity.

An example of the optimization procedure is given below by the computer output (Table 12) for the design of cyclone T-2A. In this case the minimum value of ξ^* occurs for R = 3 and H = 23. However, by accepting slightly less (6%) than optimum performance, a shorter and therefore more easily constructed cyclone is obtained by using R = 3.5 and H = 13.

Table 13 gives the values of important parameters for the three cyclone types designed by this method.

3.6. Experimental evaluation of a sampling cyclone

The TVA field trial was the first experimental test of the optimization process as applied to small cyclones. A high efficiency cyclone designated T-1A was designed and constructed for the test. The important dimensions for this cyclone are listed in Table 14. Since λ is dependent on the Reynolds Number in the cyclone, both λ and U vary with flow. Cyclone T-1A was designed during the early development stages of the optimization procedure and as a result of some errors the cyclone is not optimum. The value of α' was assumed to be 1 based on past experience with cyclones having R = 3; however, this is not accurate for R = 8. Actually α' is less than 1 and thus the indicated inlet radius is far too small.

Table 12. The computer printout for the optimization calculations for cyclone T-2A. The numbers inputed after the question are the values of R, B*, λ, and ($H-H_i$). The five columns of output are the values of H scanned and the corresponding values of the parameter ξ^*, the dimensionless pressure drop ζ, inlet ration A_o' and peripheral velocity U.

What are R, B, Lambda, and $H-H_i$ (must be < 5) ? 2.5, 1E-4, .038, 4

H	XI* x 10^4	Zeta	FA'	U
5	1.9	******	-.195	8.944
21	1.7	25.327	.367	1.059
23	1.5	19.858	.428	.957
25	1.4	16.249	.489	.873
27	1.3	13.729	.550	.803
29	1.2	11.893	.611	.743
31	1.2	10.503	.671	.691
33	1.1	9.435	.732	.647
35	1.1	8.584	.792	.607
37	1.1	7.897	.853	.572
39	1.1	7.333	.913	.541

What are R, B, Lambda, and $H-H_i$ (must be < 5) ? 3, 1E-4, .038, 4

H	XI* x 10^4	Zeta	FA'	U
5	3.3	******	-.168	7.454
11	1.9	40.734	.325	1.899
13	1.4	23.665	.465	1.541
15	1.1	16.485	.602	1.297
17	1.0	12.679	.738	1.121
19	0.98	10.375	.873	.987
21	0.96	8.854	1.007	.882
23	0.95	7.787	1.141	.797

What are R, B, Lambda, and $H-H_i$ (must be < 5) ? 3.5, 1E-4, .038, 4

H	XI* x 10^4	Zeta	FA'	U
5	8.0	******	-.117	6.389
7	4.5	******	.192	3.117
9	1.7	32.064	.447	2.130
11	1.2	17.941	.687	1.628
13	1.1	12.563	.921	1.321
15	1.0	9.814	1.152	1.118
17	1.0	8.177	1.381	.961

What are R, B, Lambda, and $H-H_i$ (must be < 5) ? 4, 1E-4, .041, 4

H	XI* x 10^4	Zeta	FA'	U
5	15.0	******	-.104	5.590
7	3.2	59.925	.318	2.728
9	1.6	21.321	.671	1.863
11	1.3	13.152	1.004	1.425
13	1.2	9.741	1.329	1.156
15	1.2	7.909	1.650	.973

Table 13 Cyclone Dimensions

Parameter	Cyclone Type		
	T-1B	T-2A	T-3A
B*	2.5×10^{-5}	10^{-4}	7.5×10^{-4}
ξ^*	6.2×10^{4}	1.1×10^{4}	1.3×10^{3}
R	7	3.5	2
H	17	13	7
$A_{\alpha'}$	2.167	0.921	0.822
u	0.961	1.321	1.992
ζ	12.56	15.45	
h_1	0.306	0.826	2.708
h_2	0.996	1.859	2.031
h_3	0.230	0.620	2.031
h_4	—	—	1.720
r_1	0.080	0.198	—
r_2	0.077	0.207	0.677
r_3	0.536	0.723	1.500
r_4	0.092	0.250	0.677
b	—	—	0.750
θ	24°	14°15'	22°

Table 14 Parameters for cyclone T-1A with Q = 1 cfm

H = 15	r_3 = 0.559"
R = 8	r_2 = 0.070"
Hi = 11	r_1 = 0.177"
U = 1.133	h_3 = 0.209"
$B = 2.5 \times 10^{-5}$	h_2 = 0.768"
λ = 0.040	h_1 = 0.279"
A = 2.24	θ = 31°

The results and procedures for the TVA trials are fully reported elsewhere. The theoretically predicted cut-off point was 0.43 μm and 1 cfm with a pressure drop of 33.6" of H_2O. The actual values achieved were 0.74 μm and 26" of H_2O. The possible causes for this descrepancy are two-fold. According to theory and the measurements of Muschelknautz, the cut-off point of the cyclone varies with $(1/r_2)^{0.5}$. These reported measurements were made for cyclones having values of R = 2 to 4. In data obtained by First for cyclones with R = 1.5 to 3, the total mass efficiency for a cyclone varies with $(1/r_2)^{0.2}$. However, these two results are not directly comparable because of differences in the way cyclone performance was measured. It is possible however that beyond some point an increase in R (smaller r_2) will not actually produce a proportionate increase in efficiency as predicted by theory. Measurements of cyclone T-2B with R = 3 will reinforce this point.

Another difficulty is the undersized inlet pipe. Since α' is smaller than assumed, A and therefore r_1 must be larger to obtain the optimum value of $A_{\alpha'}$. The smaller r_1 causes the inlet velocity to be much higher than required. Ideally, the inlet velocity should equal the peripheral velocity, u_i, of the vortex which is set primarily by r_3 and Q. The flow in the cyclone will be undisturbed if these conditions are set. It may be possible that the increased inlet velocity produces enough turbulence to reduce the efficiency of the cyclone. The lower than predicted pressure drop in the cyclone may indicate that this is not the case since increased turbulence should increase the pressure drop.

A theoretical evaluation of the effect of increasing the wall friction, λ, indicates that this factor alone cannot account for the reduced pressure drop. However, as pointed out earlier, λ was found to be a function of wall roughness in these small cyclones. The measurements of Muschelknautz show that λ is only a function of Re_R when $Re_R > 100$. Even at a flow rate of 1 cfm, $Re_R = 28.5$ for cyclone T-1A.

A measure of the steepness of the collection efficiency curve for a device is given by the geometric standard deviation of the collection efficiency S where

$$S = \frac{\text{Particle diameter at 50\% efficiency}}{\text{Particle diameter at 84.13\% efficiency}}$$

We are pleased to reveal that the optimization procedure for the cyclone design produced a very steep efficiency curve having a geometric standard deviation of 0.94. This

surpasses the performance reported for several cyclones[17,18,19] as well as for inertial impactors[20].

4. Review of Laboratory Equipment

4.1. Wind tunnel and laboratory preparation

Several modifications were made to the wind tunnel after it was moved from Gainesville, Florida and reassembled in our facility at 2600 South Michigan Avenue, Chicago, Illinois, to allow better performance (see Figure 18). The sections of wind tunnel are supported by small screw jacks and sealed together using silicon rubber o-rings. Two difficulties in tunnel operation were experienced in Florida:

1) to obtain low velocities in the wind tunnel, the opposed vane damper had to be shut completely which caused high particle deposition on the damper, and
2) short-term variations in air velocity in the tunnel interfered with turbulence measurements.

An old auto transmission was therefore modified and connected to the fan drive to allow a reduction of air velocities without the use of the damper (see Figure 19). In addition, to determine the source of the velocity variations, a tachometer was installed on the prop to measure prop speed. The two highest gears in the car's transmission produced velocities of 4372 and 3012 feet per minute at room temperature. Using the tachometer, we determined the prop speed in high gear varied from 1880 to 1876 rpm in a period of from 5-8 seconds. This corresponded to a velocity variation of 53.9 to 54.6 miles per hour at room temperature and accounted for approximately half of the velocity variations encountered in Florida. The other half was due to temperature variations caused by the large dead band in the temperature controller used on the heat exchanger. A new solid-state temperature controller was installed which reduced the temperature dead band from 10°F to 1°F. The old controller has been installed as a redundant safety device and senses the temperature inside the heat exchanger by turning off the gas supply and setting off an alarm whenever the heat exchanger rises above its safety limit, 550°F. This prevents burn out of heat exchanger even if the gas supply is accidentally left on after the wind tunnel has been turned off. A second solid-state temperature controller has been installed

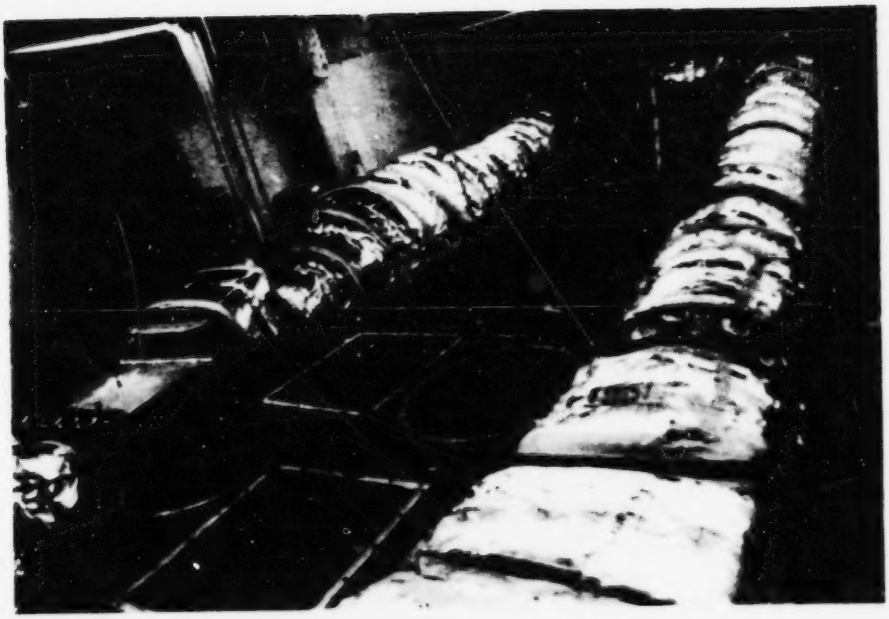

FIGURE 18 Overall view of the wind-tunnel test facility

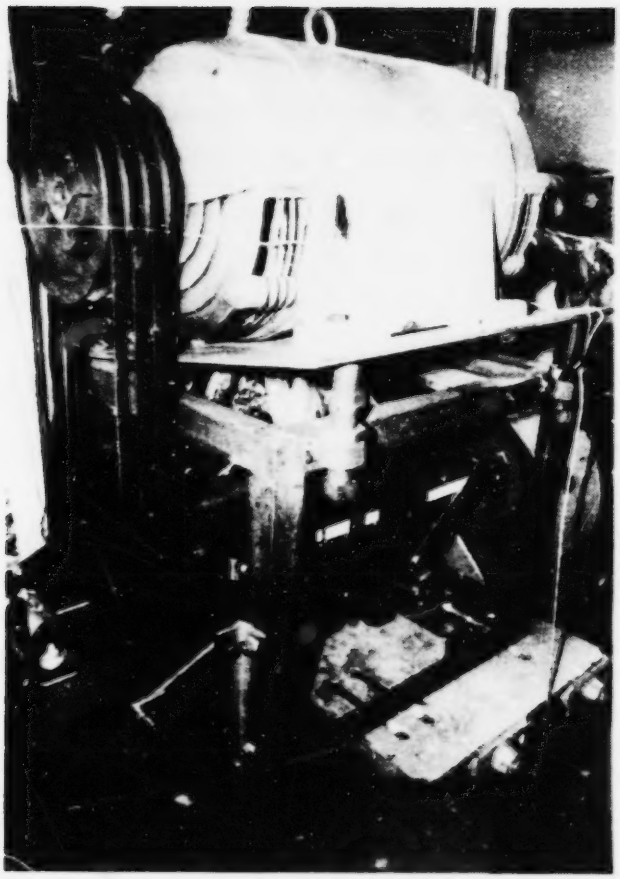

FIGURE 19 Modified auto transmission installed on the wind tunnel

as a dew point sensor to control humidity in the wind tunnel. The dew point sensor is an ordinary thermal couple surrounded by glass wool which is soaked in water from a small reservoir. Air from the wind tunnel is withdrawn by a small probe and blown over the wet bulb. The dew point in the wind tunnel is controlled by regulating the amount of water fed into the tunnel from a small reservoir with a solenoid valve controlled by the dew point sensor. The amount of water which must be added to the wind tunnel to obtain the conditions that will exist at the scrubber of the TVA has been calculated and is shown in Table 15.

Table 15 Amount of water required to maintain a given humidity in the wind tunnel

Position	Dry Temperature (°F)	Wet Temperature (°F)	Relative Humidity (%)	Amount of Water Required (ml)
Inlet	300	112	1.76	257
Outlet				
before reheating	128	124	90.5	570
after reheating	250	137	7.73	612

The particulate concentrations which occur at the scrubber site will be simulated in the wind tunnel by adding glass beads. The amount of glass beads required to obtain the expected dust loadings are detailed in Table 16.

Since the size-selective sampler will be calibrated using microscopic techniques counting single particles, it is important that the glass beads enter the sampler as single particles and not as agglomerates. Agglomeration causes errors in the collection efficiency calibrations and occurs for particles smaller than 5 μm due to electrostatic charging. A bi-polar ion generator described by Whitby[21] has been added to the wind tunnel to neutralize electrostatic charges on the particulate matter. This device uses a Corona discharge to create an air jet containing 10^{+11} bi-polar ions/cm^3 which are injected into the wind tunnel.

Table 16 Amount of flyash and limestone required in the wind tunnel to maintain a given particle concentration

Condition	Inlet		Outlet	
	Particulate Concentration (lb/ft^3)	Weight of flyash and limestone needed (g)	Particulate Concentration (lb/ft^3)	Weight of flyash and limestone needed (g)
0% excess limestone injection	8.2×10^{-4}	93	8.35×10^{-6}	0.95
0% excess dolomite injection	7.8×10^{-4}	88	7.23×10^{-6}	0.82
150% excess limestone injection	1.3×10^{-3}	147.5	1.22×10^{-5}	1.39
150% excess dolomite injection	1.2×10^{-3}	133.6	1.11×10^{-5}	1.26

Two difficulties in obtaining a satisfactory sample of glass beads have been encountered and solved. The beads obtained from a manufacturer must be separated to obtain uniform density by using the density gradient tube. The density gradient separation technique developed during a previous contract had to be modified because absorbed vapor on the glass beads altered the density of the tube and a gradient could not be maintained. Oven drying the beads removed the absorbants.

We also found that these beads contained no particles smaller than 0.9 μm in diameter. A sample of glass beads was purchased from Particle Information Service which contained a large number of submicrometer particles, the smallest of which is 0.3 μm in diameter. A spinning riffler was designed and constructed to produce a uniform mixture of glass beads. The riffler was constructed from a discarded rotating display table and seven pie-shaped plastic dishes. A vibrating hopper filled with glass beads feeds the material into the pie-shaped dishes which are rotating beneath the hopper.

Since the size resolution of most size-selective sampler is quite high, it was necessary to improve the Climet light scattering particle counter for sampler testing (see Figure 20). The resolution was improved in two ways: the old tungsten filament light source has been replaced by a quartz iodine lamp with about twice the illumination and a new photomultiplier high voltage power supply has been installed with a far better voltage stability than the old supply. These modifications reduce the signal to noise ratio and therefore improve the size resolution by a factor of 3. The orifice in the sampling section of the Climet has been increased from 0.42 to 0.72 inches in diameter to allow use of the Climet at flow rates of 0.8 cfm.

Since we found that optical microscopy could not be successfully used with the automatic image analyzer for particle size distribution analysis in the submicrometer range, it was necessary to construct an epidiascope attachment for the analyzer to view photomicrographs taken with the scanning electron microscope and determine the particle size distribution of the particles in the micrograph. The epidiascope uses a 50 mm camera lens to image 35 mm negatives on the face of the TV camera tube. The 35 mm negatives are held in a special negative carrier and illuminated by transmitted light. A size standard is included on each film roll taken with the

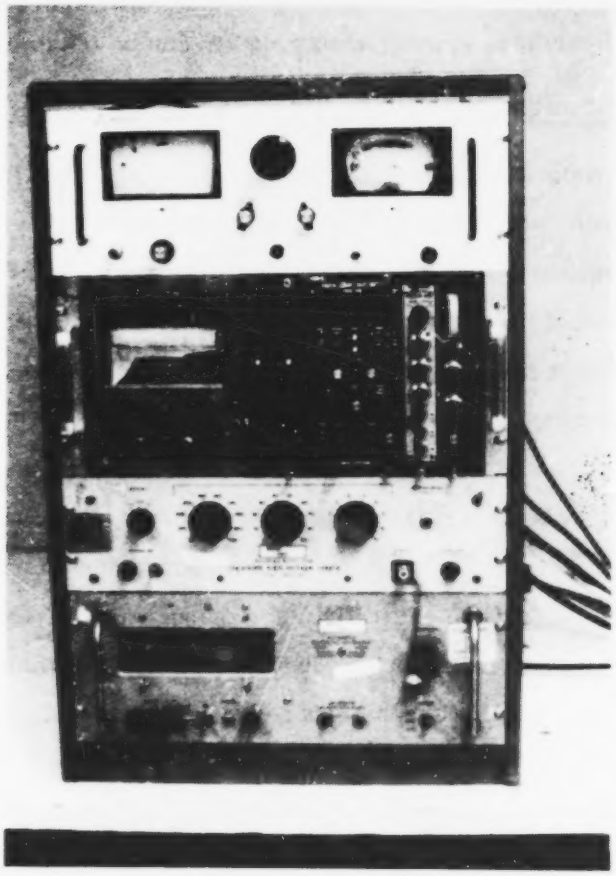

FIGURE 20 Climet light-scattering particle counter with the new photomultiplier power supply and a digital volt meter for setting precise discriminator levels

scanning electron microscope and allows calibration of the ΠMC and eliminates the source of inaccuracy. Any size standard can be used, but for these analyses we used a 5 μm diameter electron microscope aperture. A prime calibration of the SEM is made using a replica diffraction grading of known accuracy. In this way size distributions of particles greater than 0.05 μm can be obtained with an accuracy of ±5%.

4.2. ΠMC evaluation

As was reported in our March progress report, the ΠMC automatic image analyzing computer was ordered and installed in March.

The computer was connected to a Leitz research polarizing microscope equipped with a special set of plan apochromat objectives. This scope allowed the computer to resolve details in the sample much better than would be possible with ordinary achromats or fluoride objectives.

So that the instrument could be evaluated correctly, we prepared several different type samples in several different mediums. Each sample was counted several times and finally the same areas were sized and compared. Different types of illumination—bright field, dark field and monochromatic light—were also used.

Through experimentation we found that the best medium is a viscous liquid with a high refractive index (n); but yet relatively inert and noncorrosive.

The best medium was Aroclor®5442, a chlorinated polyphenol resin manufactured by Monsanto Laboratories. The refractive index is 1.662 which is actually not high enough for this type sample. We have found that the small particles, less than 0.5 μm, cannot be detected by the computer because the light rays are not diffracted enough to provide good contrast between the particle and background light.

Statistically the ΠMC unit has an overall accuracy of about 7% and this is only achieved under good sample preparation techniques.

Because the system is connected to a light microscope, there is automatically a 1-3% increase in the particle size due to the diffraction rings surrounding the particle. However, these diffraction rings prevent a perfect image at the edge of the particle. There is no way to negate these rings without losing the image quality required to activate the automatic image analyzer. With good plan aprochromatic

objectives and low magnification, these rings are reduced in size with a 0.5-1.0% increase in size of the particle and with good plan aprochromatic objectives and high magnification the size increase is 1-2%, and with an achromat objective the increase is 3-4%.

Another factor which must be considered is the sample preparation. The samples for analysis must be taken from different areas of the filter so that the cumulative sample analyzed is as accurately representative as possible. The computer contains a built-in particle size discrimination factor. Line voltage variation, internal binary noise, discriminator settings and operator error add together another 3% to the total of 7%.

One of these problems we have been able to eliminate. By using a scanning electron microscope (SEM) for the image requirements, the associated error reduces to less than 0.25% for the image requirements.

5. Field Test: Kansas Power and Light Company

5.1 Background

The Kansas Power and Light Company (KPL), Lawrence, Kansas, uses a pulverized coal boiler with injected limestone and wet scrubber to control SO_x emissions. This unit, designed by Combustion Engineering, Inc., was under test by APCO's division of compliance, Durham, North Carolina. Emissions testing for compliance was performed by York Research on 22-26 March 1971. Waldon Research also had permission to test SO_2 monitors the same week we performed our experiments.

5.2. Experimental plan

Our experiments were planned to obtain:

1) The amount of particle deposition in sampling tubes as a function of their size and flow rate,
2) changes in particle mass and size distribution due to an isokinetic sampling,
3) the accuracy of the Andersen Stack Sampler as a size selective impactor, and
4) the size range efficiency of two cyclone samplers.

5.3. Description of KPL tests

5.3.1. Time priorities

R. Battles, H. Humecki and T. Smith of McCrone Associates met with Mr. J. Rohm of APCO, coordinator for all testing, and Mr. M. Funston, plant manager for KPL, 22 March 1971 at KPL. Mr. Rohm informed us that York Research would test at both scrubber outlet stacks, occupying all the sampling ports all day Tuesday and until noon on Wednesday and Thursday. Walden Research would be sampling the inlet during this time and the outlet on Wednesday, Thursday and Friday afternoons, simultaneously with us, and at noon on Friday the unit would be switched from coal to gas.

This allowed us a day and a half at the outlet and two days at the inlet. Our original sampling time plan required three days at the outlet with a day and a half at the inlet. This time discrepancy plus several equipment breakdowns cut heavily into completing all the planned tests.

5.3.2. Completed tests

The sequence of tests were arranged to conform to the time available. Our tests and operating experiences are described below in chronological order.

(a) Tuesday—cyclone samplers at inlet

Our sampling train consisted of two external cyclones in series, followed by a filter. We intended sampling the scrubber inlet for one hour with this train, using a one-half inch diameter nozzle and probe at a 5.5 cfm sampling rate. The nozzle diameter and sampling rate were chosen—based on our preliminary dust deposition data—to minimize particle deposition in the probe. At this sampling rate the large cyclone would have a 50% collection efficiency of 5 microns and the second cyclone would collect particles down in the submicron size range. Both these cyclones and the filter holder were placed inside the sampling box on loan from APCO. For a water trap, we connected a heat exchanger, three bubblers and a silica gel trap in series. A 5 cfm carbon vein pump was followed by a dry gas meter and a calibrated orifice meter.

The ducts to the sampler scrubber inlet were horizontal and, since there

was no room to insert the probe into the side of the duct, dust collection with the cyclones could not fall into the collection pots; but instead remain inside the cyclones. This consequently caused a re-entrainment of the particles collected. Since our large cyclone was designed for laboratory use, it is actually inconvenient for field use because of the method for fastening the cover. If it is necessary for a cyclone to be taken apart for cleaning, an easily removable clamp should be used to hold the cyclone together, We obtained a 49-minute duration cyclone and back up filter sample from the inlet.

Several other minor problems were encountered; these resulted from the design of these particular cyclones. The pressure drop across the sampling train was so great that it was impossible to sample at a rate greater than 2.5 cfm. Another problem was that our freon cooled heat exchanger plugged with ice due to high humidity of the inlet gas. Also, the swivel adapter connecting the 0.50 inch probe to the 1.0 inch inside diameter cyclone inlet caused significant deposition at their junction. A considerable quantity of dust deposited immediately before the adapter. Also, the transition from the very large outlet diameter of the first cyclone to the small inlet diameter of the second cyclone caused some deposition. The practice of using a probe nozzle whose diameter is smaller than the transport tube diameter causes increased dust deposition in the tube, and should not be used for accurate sampling. This dust deposition is mainly due to the decreased velocit through the carrier tube.

(b) Tuesday—Andersen Sampler at the inlet

After we had completed sampling with the series cyclones, we connected the large cyclone in front of the Andersen sampler. A 0.25 inch inside diameter probe was used with a 0.75 cfm flow rate to minimize deposition in the sampling tube. We attempted sampling with this train at the scrubber inlet, but the large cyclone came apart. As a result, further attempts to sample with the large cyclone at the scrubber inlet were abandoned.

(c) Wednesday—Andersen sampling at outlet

Wednesday afternoon we were able to move our equipment to the scrubber outlet and begin sampling with the Andersen Stack Sampler. The sampling train consisted of a 0.25 inch probe and nozzle connected to the inlet of the Andersen Sampler followed by a filter and two heat exchanger cyclones to remove water vapor. The heat exchanger cyclones were cooled with a bottle of freon. The sampling port and position we used was the same as port number 3 sampled by York Research, and was 23.6 inches inside the stack.

The Andersen Stack Sampler was used for three sampling times: 1, 4 and 10 minutes at a flow rate of 0.75 cfm. Several difficulties were encountered in sampling with this train. The Andersen Sampler and back-up filter were heated with temperature controlled heating tapes and since the sample box had no thermal baffling, it was necessary to surround the impactor and filter holder with glass fiber insulation to prevent overheating the other components in the sampling box. Since the heating tapes were secured with metal clamps, it was cumbersome removing the tapes from the then hot components so the impactor plates could be removed. Also the thermal couple for the temperature controller was located at the outlet of the filter holder. As a result, unless gas is coming through the filter holder, the thermocouple is isolated from the Andersen impactor and filter holder. Thus, the temperature of the impactor and filter holder will be considerably higher than the set point of the temperature regulator. The 0.25 inch diameter probe used for sampling with the impactor was cleaned between each of the three runs and little deposition was observed.

The small cyclone heat exchanger froze and plugged during the four minute sampling run, necessitating a rerun. Although the gas temperature stayed between 30°F and 40°F, the small inlet diameter caused the plugging, since the freon flowed through the small (second) cyclone cooling jacket and then through the larger cyclone heat exchanger. The two cyclones were connected in series, both for freon coolant and for sampling gas, however, it was impossible to maintain a temperature in the first cyclone lower than 100°F, even when the second cyclone indicated a temperature of 30°F. The cooling jackets should have been connected in parallel. Alternately, a

higher boiling freon could be used to prevent clogging the heat exchangers. The life of the 12 pound freon bottle was roughly one sampling hour.

Upon changing the impactor plates, we observed that the particles formed small mounds just below each jet. Each plate was placed in a petri dish along with its spacer ring for transport for lab analysis. This method of packing the particle loaded plates is not oompletely satisfactory since some of the particles could be dislodged during transportation. If time permitted, a transporter container could have been made to hold the entire set of plates and spacers similar in a way as they are held in the impactor.

(d) Thursday—Particle deposition in probes at the outlet

On Thursday morning the sampling trains were assembled so that two deposition studies could be performed. Two large filter holders were placed side by side in the APCO sampling box and the probes were connected to the filter holders with swagelock fittings. One sampling train consisted of the APCO pump and dry gas meter, while the other was a standard RAC train. Two bubblers, connected in series, were used in each train to remove water vapor. By Thursday afternoon York Research had completed their sampling and we had completed assembly of the two sampling trains. We attempted to calibrate the orifice meter in the APCO train, but the dry gas meter failed. After some searching we were able to find a small wet test meter that Combustion Engineering had used, and we then finally calibrated the orifice meter at 0.75 cfm. As a result of the dry gas meter failure, we were not able to accomplish any simultaneous iso- and aniso-kinetic sampling Thursday.

The week before our field sampling we tested the dry gas meter in the APCO train and determined that it was in error by 2.5%. We also discovered two leaks in the APCO train which were corrected. It was necessary to operate the RAC unit some 30-60 minutes in the field to free the dry gas meter in that train. This problem has never been observed in the lab, but only occurs when temperatures are low, but still above freezing.

(c) Friday—Particle deposition in probes at the outlet

On Friday morning we started early and were able to perform a number of probe deposition studies. One tube was used at a flow rate of 0.75 cfm at position number 3 in the stack for a sampling time of 30 minutes. One filter sample was also collected using a 0.375 inch diameter probe at the flow rate o. 3 cfm and a sampling time of 30 minutes. Since this filter sample was fairly representative of the particles in the stack, it was used to determine the particle size distribution.

5.4. Series cyclone efficiency

As we have already discussed, only one 49 minute test run was completed with the series cyclones at the inlet on Tuesday since we found that the system had several problems—one of which is design. The cyclones were designed to be used in an upright position during the sampling. However, since the inlet port was on top of the duct, it was necessary to lay the sampling train on its side. As a result we found a great amount of particle deposition inside of each cyclone. The transport tubes and connections also aided in particle deposition. This allowed particle re-entrainment and reduced the cyclone's efficiency. Nearly all of the small particles were allowed to pass through as well as some of the large particles.

We have reached these conclusions by direct observation of the deposition and a comparison of the laboratory tested efficiency of 85% and the less than 30% efficiency found in the KPL test.

From these conclusions we feel that the field test efficiency could have been increased to a realistic efficiency given more time to better prepare ourselves about the actual source.

5.5. Probe deposition

On Thursday and Friday we performed tests with four probes of different diameters to learn about probe deposition. As we had learned from our laboratory tests, particle deposition is decreased as the probe transport tube diameter decreases.

This was found to be true in the field test at KPL when the tubes are horizontal. We also found that there is an increased particle deposition when the same tube is held vertically. The highest efficiency obtained was with a small transport tube used with the proper nozzle diameter and held in a verticle position during sampling. The efficiency was determined to be approximately 98% for a 0.25 in tube held horizontally and 87% for a 0.50 in tube which held vertically.

6. Field Test: Shawnee Power Plant

A field test of the small cyclone was carried out to prove the viability of cyclones as size selective samplers. The test was conducted on the Zurn pilot plant scrubber connected to unit 10 of Tennessee Valley Authority's Shawnee Power Plant. The pilot plant is a cyclone and scrubber connected in series to the precipitator inlet. During the tests limestone was injected into the boiler at a stoichiometric ratio of 1 to 3.

All our sampling was done using a standard RAC sampling train at the outlet of the scrubber (see Figure 21). A special 3/8 in I.D. x 2 ft long stainless steel, heated probe was used to heat the gas to 275°F before it entered cyclone T-1A. The dimensions of this brass cyclone are given elsewhere in the report. The particles escaping the cyclone were collected on a 90 mm, 0.25 μm, Solvinert filter. These filters were selected for evaluation because of the high tare weight and their ability to withstand high temperatures. The cyclone and filter holder were housed in the RAC sample box and heated to 275°F during sampling to prevent water condensation. Small pressure taps were connected to the inlet and outlet of the cyclone so that the pressure drop could be monitored while sampling.

Several samples were collected, but were later discarded because of equipment malfunctions. Another problem encountered was the short running time of the scrubber during most of the experiments. One sample was successfully taken which allowed an evaluation of the cyclone's performance. During this sample the stack gas was 127°F, contained 9.70% water vapor by volume and the flow rate through the cyclone was 1.01 cfm.

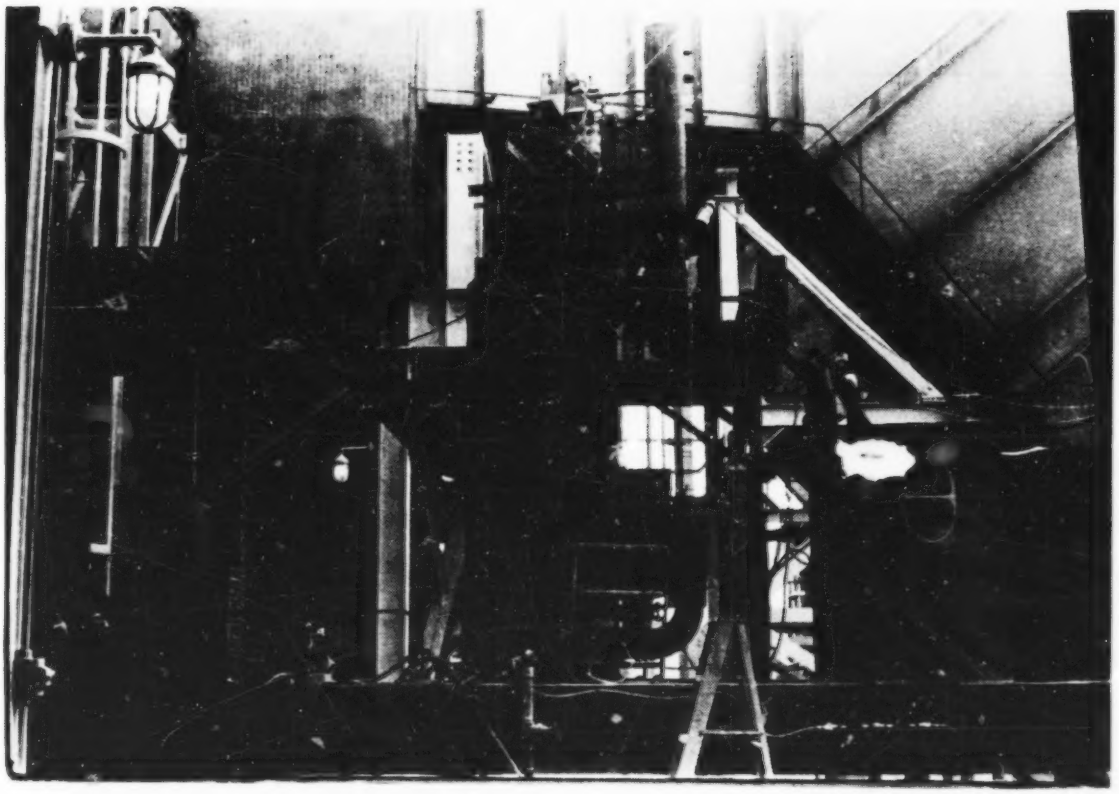

FIGURE 21 The pilot scrubber. The sampling equipment used for testing the sampling cyclone is shown at top center and bottom left.

The sample filter was dried and weighed and the particles in the cyclone were removed and weighed. The cyclone collected 17.4% of the particles. Both samples were dispersed on aluminum stubs for analysis with the Cambridge Stereoscan scanning electron microscope. A high contrast 35 mm film was used for the photomicrographs. These photomicrographs were in turn analyzed using the epidiascope attachment to the ΠMC. A calibration standard was photographed on each roll of film. The particle counts were made in groups; two hundred particles each from five portions of the sample. The five number distributions were converted to weight fractions using the geometric mean particle size of each interval. The five sets of data were averaged and the standard deviation determined. The standard deviation estimates all the errors encountered in the counting process, including random variations, operator error, and instrument variations. The results for the filter sample and cyclone catch are shown in Tables 17 and 18 and Figure 22.

Table 17 Filter catch size distribution*

Lower Size	Upper Size	Geometric Mean Size	Number Fraction	Standard Deviation	Weight Fraction	Standard Deviation
0.030	0.100	0.055	0.122	0.020	0.001	0.000
0.100	0.200	0.141	0.337	0.038	0.040	0.010
0.200	0.300	0.245	0.282	0.013	0.171	0.029
0.300	0.400	0.346	0.151	0.032	0.254	0.047
0.400	0.500	0.447	0.079	0.024	0.280	0.062
0.500	0.600	0.548	0.020	0.004	0.132	0.012
0.600	0.700	0.648	0.011	0.005	0.114	0.050
0.700	0.800	0.748	0.001	0.001	0.007	0.017
0.800	0.900	0.849	****	****	****	****

* The size distribution data and error statistics for the 1000 particles counted from the filter and cyclone catch.

Table 18 Cyclone catch size distribution*

Lower Size	Upper Size	Geometric Mean Size	Number Fraction	Standard Deviation	Weight Fraction	Standard Deviation
0.058	0.383	0.149	0.398	0.021	0.001	0.000
0.383	0.766	0.542	0.264	0.021	0.029	0.007
0.766	1.150	0.939	0.140	0.020	0.081	0.027
1.150	1.535	1.329	0.097	0.018	0.152	0.005
1.535	1.923	1.718	0.046	0.006	0.156	0.012
1.923	2.305	2.105	0.025	0.010	0.153	0.040
2.305	2.690	2.490	0.016	0.003	0.166	0.035
2.690	3.070	2.874	0.011	0.001	0.173	0.010
3.070	3.450	3.254	0.004	0.003	0.090	0.044

* The size distribution data and error statistics for the 1000 particles counted from the filter and cyclone catch.

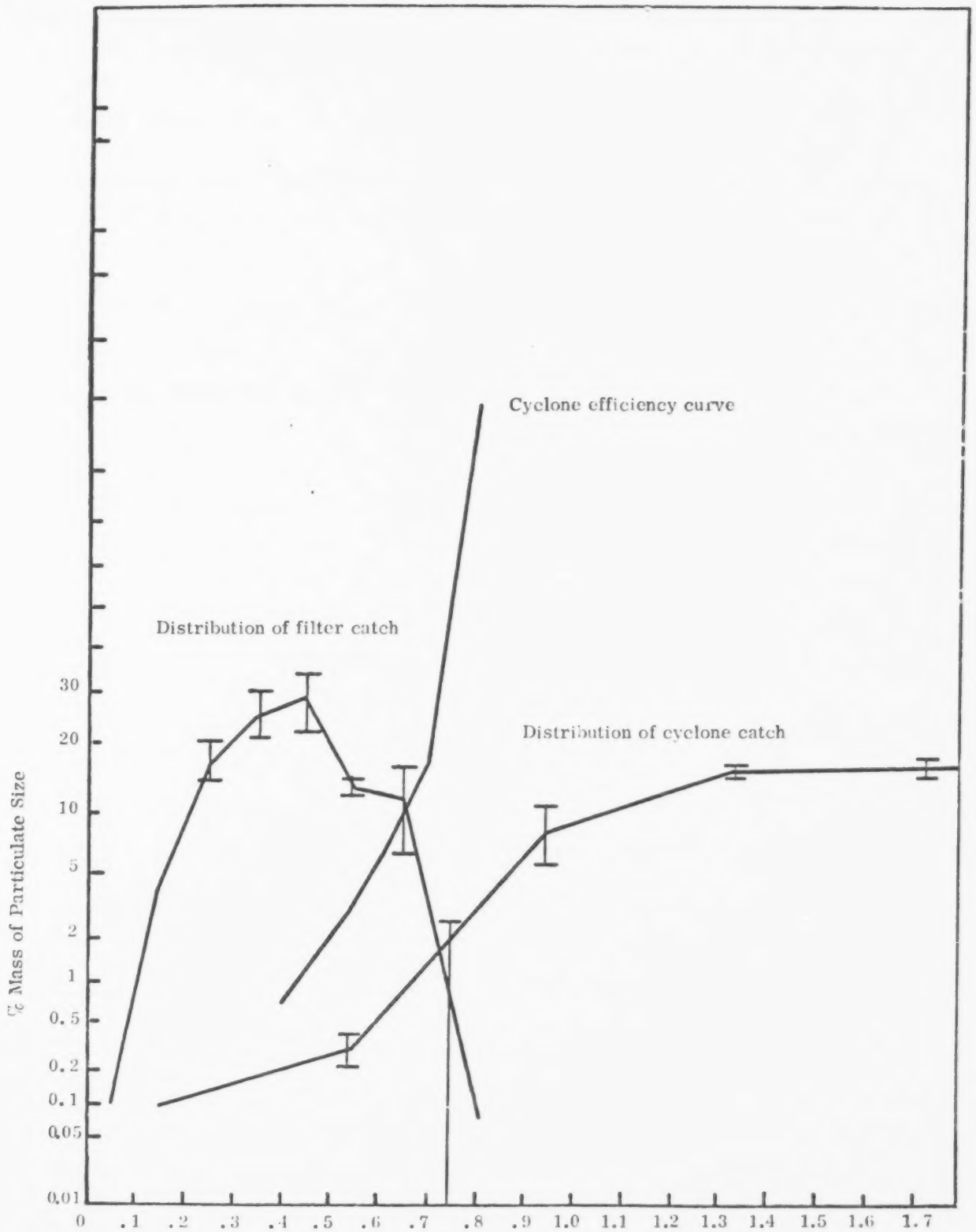

FIGURE 22 Size distribution of TVA samples collected with small cyclone

Calculating the size efficiency curve from the two weight fraction distributions is straightforward. The mass fractional collection efficiency is defined as

$$K = \frac{M_i - M_o}{M_i} = \frac{M_c}{M_c + M_o} \qquad \text{Eq. (27)}$$

Where M_i, M_c, and M_o are the masses entering, collected by, and leaving the cyclones. The fractional collection efficiency for particles of size X is defined similarly

$$E_x = \frac{X_c}{X_c + X_o} \qquad \text{Eq. (28)}$$

Where X_c and X_o are the mass of particles of size X that are collected by and escape the cyclone.

$$X_c = C_x M_c \qquad \text{Eq. (29a)}$$

$$X_o = O_x M_o \qquad \text{Eq. (29b)}$$

C_x and O_x are the mass fractions of particles of size X found in the cyclone and filter catch as given by the two mass distributions. Therefore

$$E_x = \frac{C_x}{C_x + O_x \frac{1-k}{k}} \qquad \text{Eq. (30)}$$

7. Deposition of Particles in a Horizontal Sampling Tube

Sampling errors also result from particle deposition in the sampling line down stream of the sampling probe. Therefore another problem in designing a size selective sampler is how to design a sampling line which will minimize particle deposition.

Three mechanisms contribute to the total particle deposition in a horizontal tube: diffusional deposition, gravitational settling and turbulent deposition. Each of these mechanisms is a function of several variables such as the length and size of sampling tube, sampling time, particle size and characteristics, Reynolds number of the gas, and flow rate[21].

Since many variables are involved in particle deposition, the total transport tube problem is very difficult to analyze theoretically. Therefore, empirical data will be of most value for a practical solution to the deposition problem.

The purpose of the preliminary experiment was to obtain information to serve as a guide to design a detailed field test. It is not designed to test the significance of relative effect of each variable on deposition but to observe the tendency of deposition due to variations of several important variables.

Three types of polydisperse aerosols were tested in this experiment: the mixture of flyash and limestone particles, fine glass beads and coarse glass beads. The weight average sizes of these aerosols were about 11, 24 and 85 micrometers respectively. Figure 23 shows the schematic arrangement of equipment for the particle deposition study. When each experiment was completed, the nozzle, bend and the tube were thoroughly cleaned with a specially designed cleaning tube as illustrated in Figure 24. A special tip with six 1/32 inch nozzles around its periphery was attached to one end of a 3/8 in diameter x 10 ft long tube. This end of the tube was stuck into the sampling tube and the other end was conected to the exhaust end of the pump with rubber tubing. By circulating the air through the system at the rate of about 5.5 cfm and moving the cleaning tube back and forth several times in the sampling tube, the air jet created by the nozzle was able to knock out the particles deposited in the tube. The particles trapped in the nozzle, bend and tube and collected by the cyclone and filter are respectively collected and weighed and the percentage of particles that pass through the transport tube is computed. The experiment for each aerosol was repeated several times by using various flow rates ranging from 0.7 to 5.1 cfm and two different sizes of nozzle and transport tube: 1/2 and 1 in.

In summary, the experiments were performed with the following conditions:

a. A mixture of flyash and limestone particles passing through a 1 in tube with a 90°-bend of small curvature (radius of curvature≈ diameter of tube).

b. A mixture of flyash and limestone particles passing through a 1 in tube with a 90° bend of large curvature (radius of curvature≈ 8X diameter of tube).

c. A mixture of flyash and limestone particles passing through a 1/2 in nozzle and 1/2 in tube.

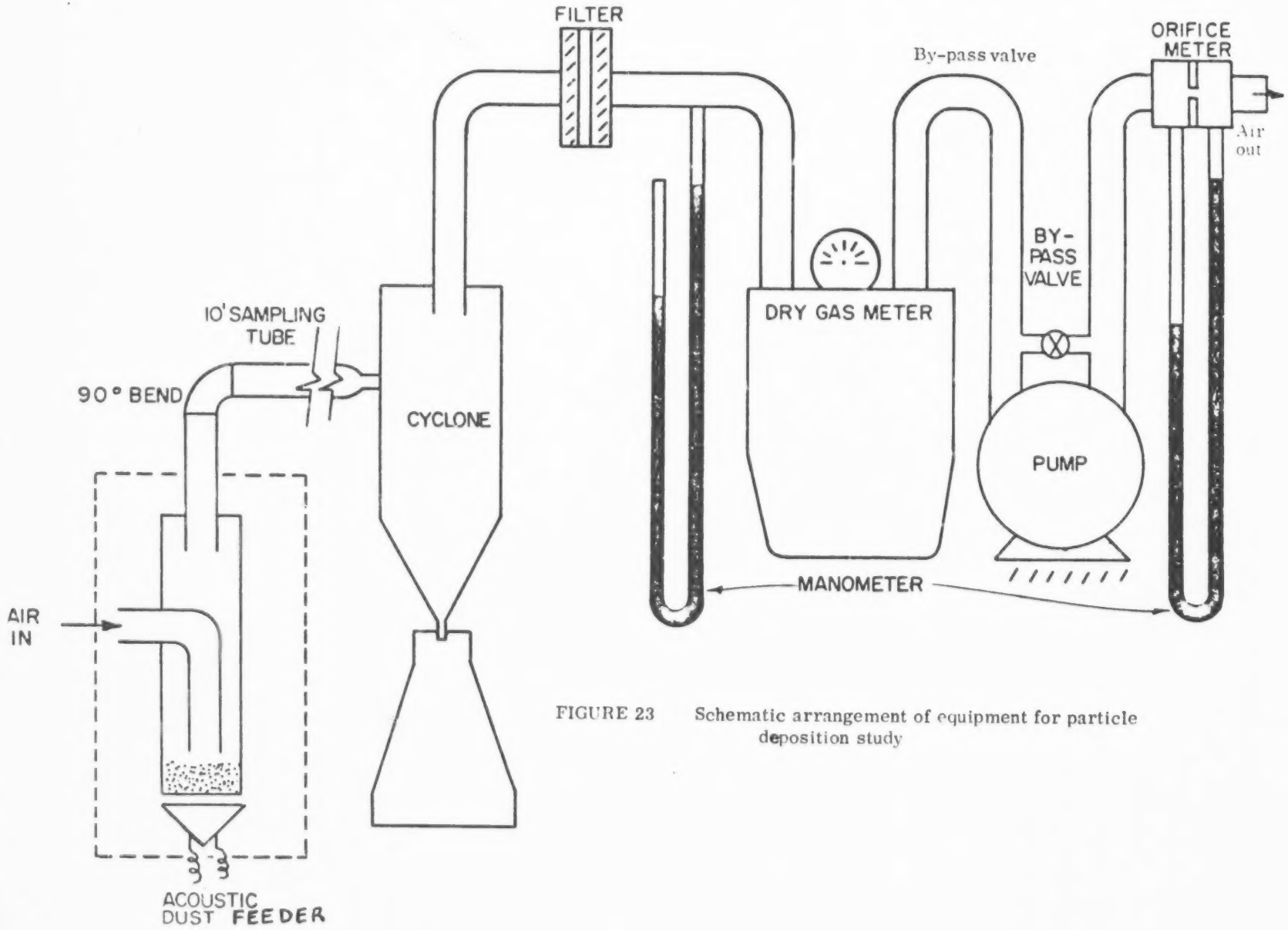

FIGURE 23 Schematic arrangement of equipment for particle deposition study

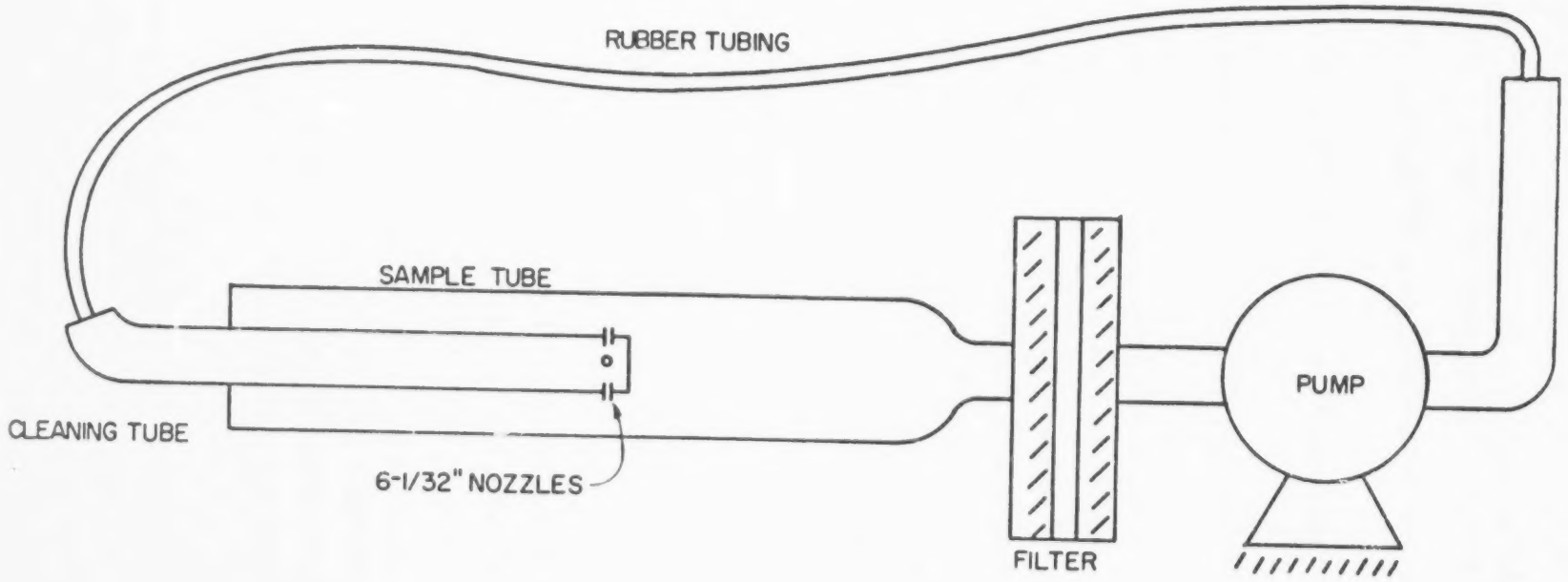

FIGURE 24 Arrangement of equipment to clean particles deposited in the sampling tube

d. A mixture of flyash and limestone particles passing through a 1/2 in nozzle, a cyclone and a 1/2 in tube.

e. Fine glass beads passing through a 1/2 in nozzle and a 1/2 in tube.

f. Coarse glass beads passing through a 1/2 in nozzle and a 1/2 in tube.

The results of the experiments under various experimental conditions are shown in Figure 25.

From these experiments we observed that for certain types of particle samples with a given sampling line the deposition increases progressively as the flow rate decreases. This is just contradictory to what Sehmel observed.[22] In his study of methylene blue-uranine particle deposition in a 10 ft vertical tube, Sehmel reports that the percent deposition within the tube increases progressively as the flow rate increases. Such differences are probably due to the differences in the adhesive characteristics, density of the particles and flow rates. Methylene blue-uranine is water soluble and has a density of 1.5 gm/cc while the glass beads and flyash are insoluble in water and have a density of about 2.5 gm/cc. The flow rates used ranged from 0.7 to 5.1 cfm and are much lower than the 0.5 to 50 cfm used by Sehmel. We also concluded from our preliminary experiment that when a 1/2-in sampling tube with a 1/2-in nozzle is used to sample the particles at the scrubber inlet, a flow rate of about 2.5 cfm is required to minimize deposition. Whereas, at the outlet about 5.5 cfm is needed. If a flow rate of 0.75 cfm is used with the Andersen Stack Sampler, as recommended by its manufacturer, a transport tube with an inside diameter of > 0.5 in should be used for minimum deposition.

The findings obtained from this preliminary dust deposition experiment were applied in our field test at KPL. A one-half inch diameter nozzle and probe were used for sampling at the wet-scrubber inlet. At a flow rate of 2.5 cfm only 4.6% (by mass) of the particles deposited in the probe with the most depositable particles in the range from 1 to 6 micrometers.

One point that deserves special mention is the segregation of particles in the sampling nozzle and the transport tube. Visual inspection of the samples collected in the deposition experiment indicates that particles trapped in the nozzle were mainly limestone and those deposited in the transparent tube were mostly flyash.

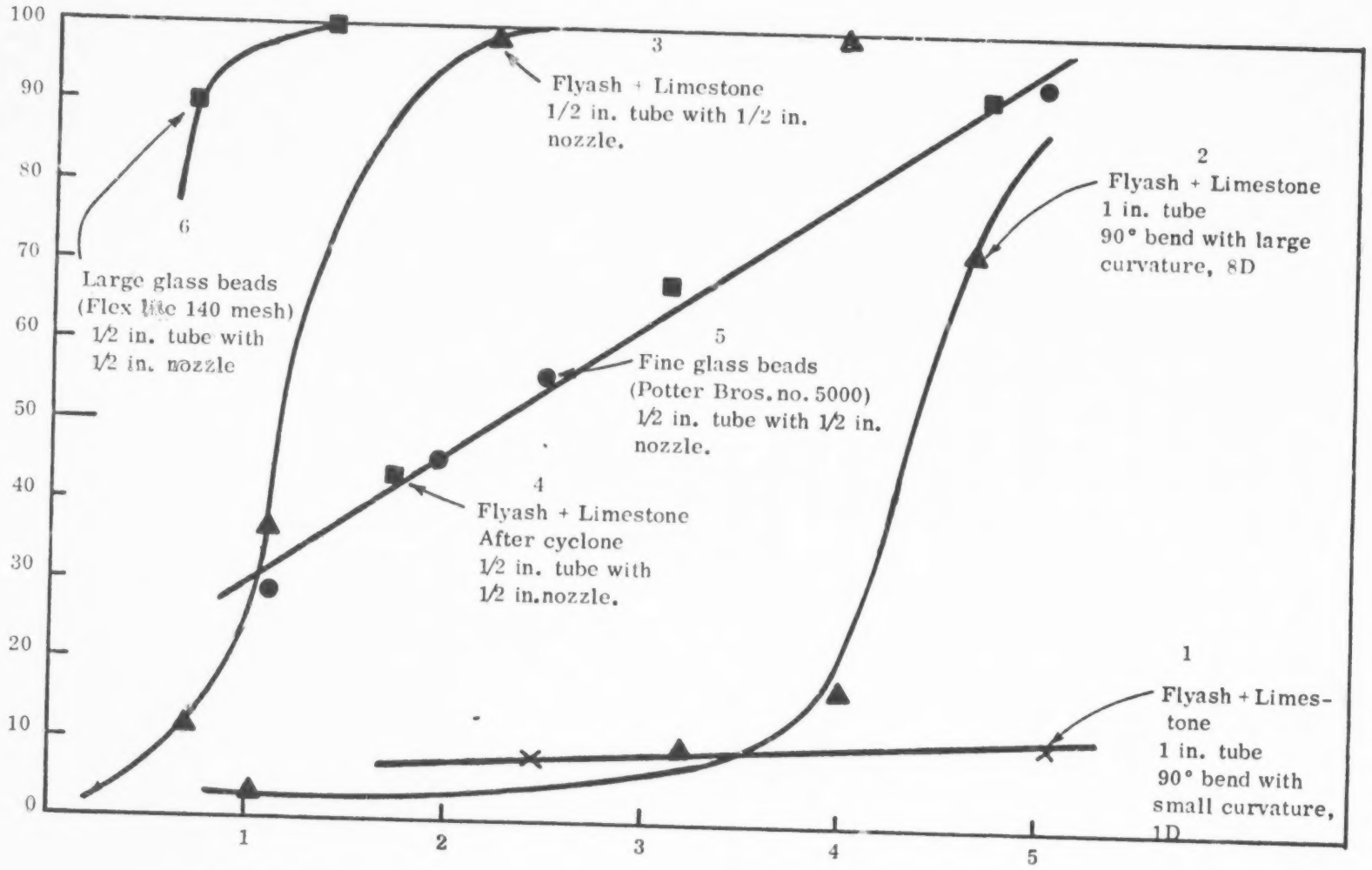

FIGURE 25 Deposition of particles in horizontal sampling tube as a function of particle size and sampling conditions

Although our preliminary experiments on dust deposition provide valuable information on the design of a sampling line, we recommend that further analyses be performed to obtain a sampling line with minimum deposition. Since porous wall tubes have been recommended by previous investigations[23], we recommend that such a tube be considered and tested. Such a tube has been obtained and a study can begin once the research funds are available.

8. Prediction of Sample Bias Due to Non-isokinetic Aspiration

For particle sampling in a stack and/or duct it is generally considered necessary to have isokinetic sampling conditions in order to obtain a representative sample. Studies on sampling bias due to anisokinetic conditions can be found in various publications[24, 25, 26]. A general conclusion from these studies is that the magnitude of sampling bias is related to particle size, diameter of sampling probe and degree of variation from isokinetic condition.

In the Bechtel report on sampling and analytical determinations for an alkali scrubbing test facility, they mention that particles larger than five micrometers do not get through the scrubber, and consequently that errors due to size classification are not introduced by anisokinetic procedures. On the basis of this information, the report concludes that isokinetic sampling is not needed at a wet scrubber outlet. In order to justify this statement and determine if isokinetic sampling is really not necessary at the scrubber outlet in this project, we performed a theoretical analysis of the predictive errors of particle sampling at the wet scrubber outlet. The mathematical model describing the sampling bias presented in our previous report[21] was used to predict the bias. The ranges of the process variables mentioned in the previous section of this report were used to compute the values of those variables involved in the model. The prediction was made for 1, 5, and 10-μm particles sampled with 1/8 and 1 in nozzles, the reasonable upper and lower limits of the proposed probe size. The results, as shown in Figures 26, 27 and 28, show the variation of nozzle bias with velocity ratio.

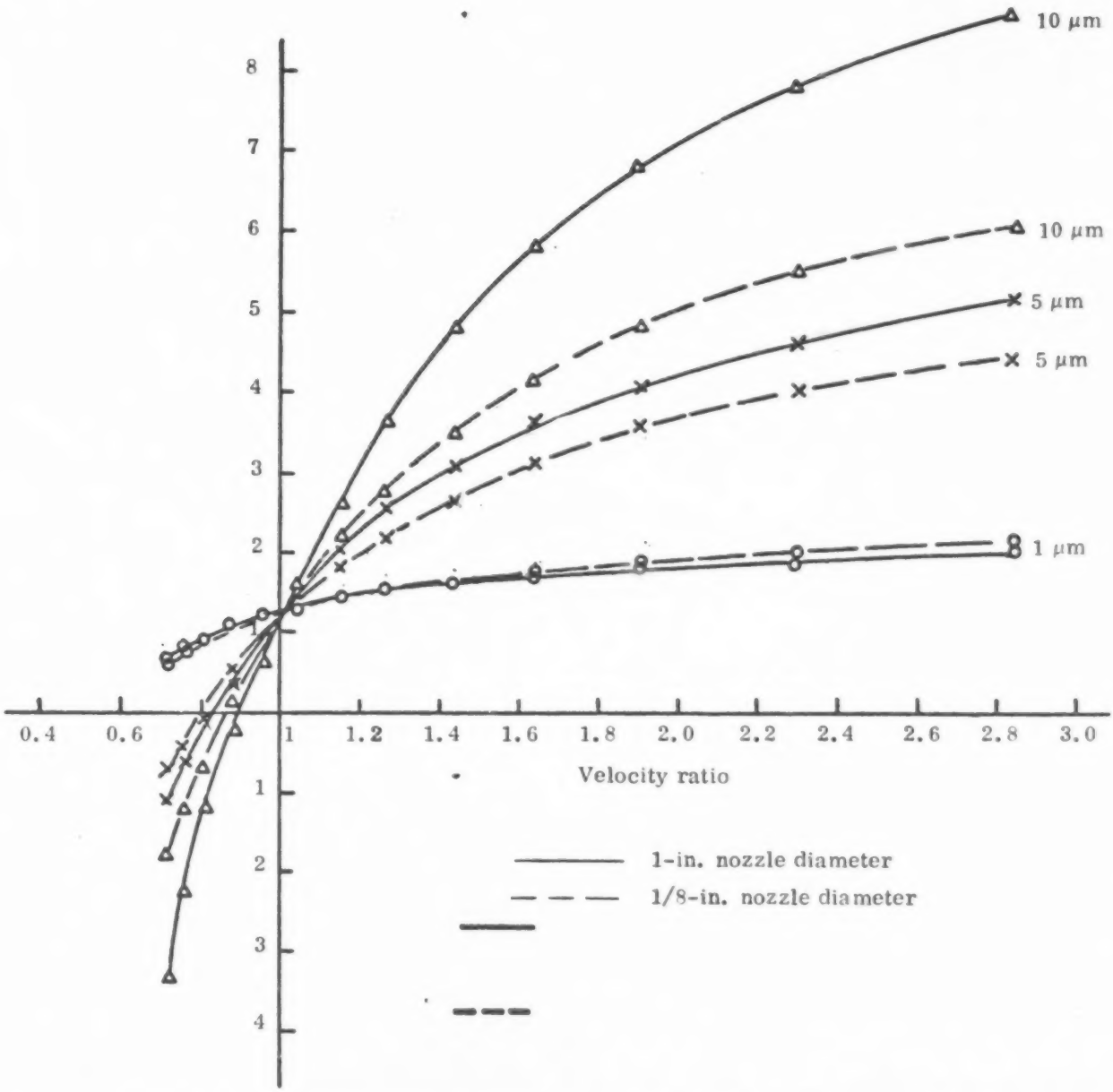

FIGURE 26 Comparison of predicted nozzle bias with the same sampling time and nozzle cross section

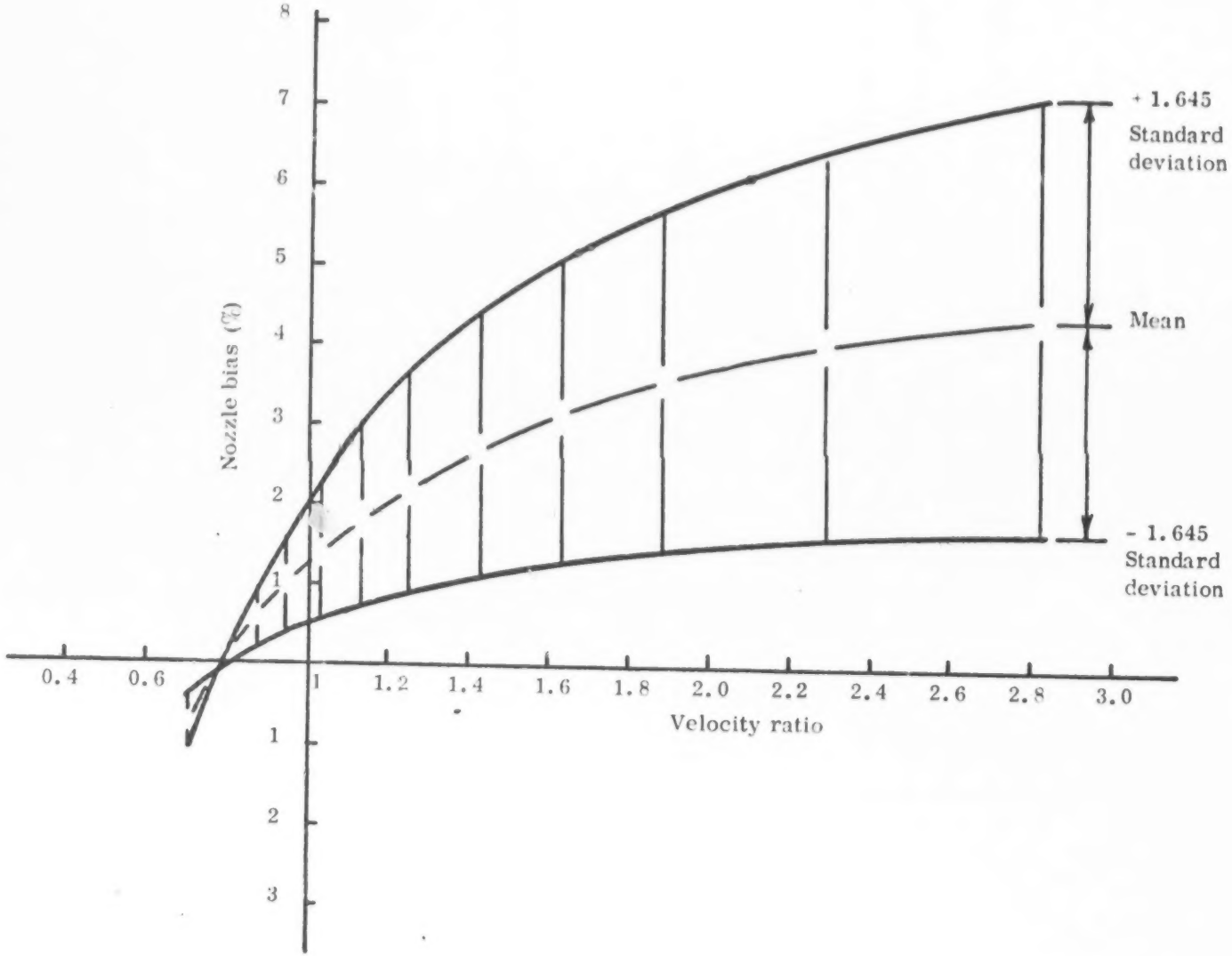

FIGURE 27 Predicted range of nozzle bias for 5-μm particles sampled with 1/8 in. nozzle at various given velocity ratios at 90% confidence level

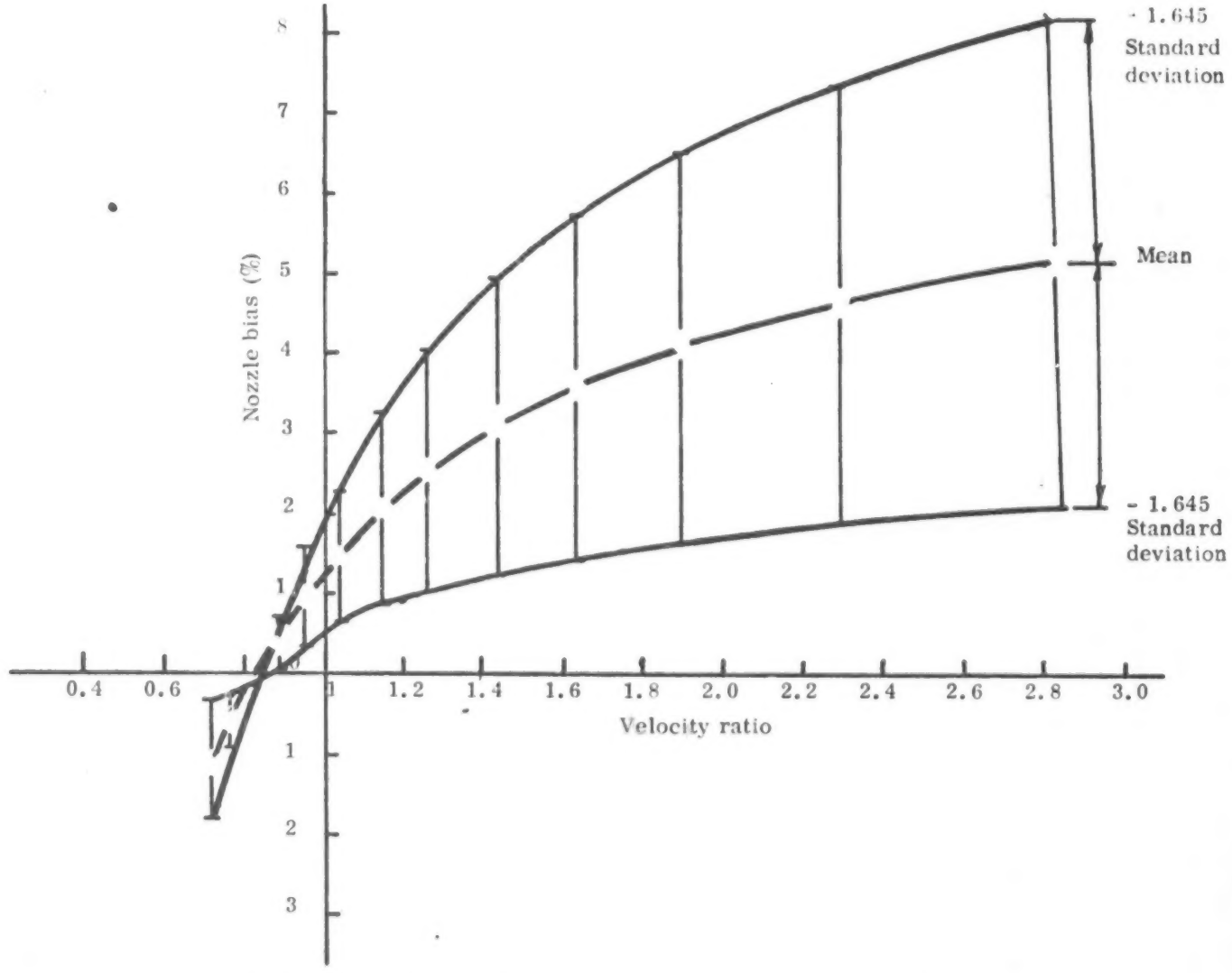

FIGURE 28 Predicted range of nozzle bias for 5-μm particles sampled with 1-in. nozzle at various given velocity ratios at 90% confidence level

Numerically, the analysis indicates that errors due to anisokinetic sampling are not very significant. For example, at the 90% confidence level the nozzle bias for 5 μm particles would be within -2 and +8.3% if one uses a 1-in nozzle with sampling velocity ranging from 0.6, and 3 times the free stream velocity. With a 1/8-in probe the bias would be much less.

The problem of whether isokinetic sampling is required at the wet scrubber outlet depends on how much nozzle bias is considered acceptable. Considering the errors introduced by other factors in sampling particles, (e.g., the readings of manometer and flowmeter scales) the error due to anisokinetic sampling may be insignificant. We concluded, therefore, that isokinetic sampling may not be needed at the wet scrubber outlet if it is proved that particles larger than 5 micrometers do not get through the scrubber and that other errors are more significant. We recommend, however, that a field test be made to test the validity of this theoretical determination.

9. Evaluation of Filters for Parallel Cyclone Samplers

Since a filter will be the particle collection substrate for the size selective sampler, filter selection is an important factor. There are several desirable qualities that a filter for this application should have. It must be able to operate at temperatures of 250-300°F, it must have a very high particle collection efficiency for submicron particles. it must withstand the attack of corrosive gases, and it must allow accurate weighing of the particles collected on the filter. In addition, a low pressure drop is desirable since this allows the use of smaller diameter filters and smaller pumps.

A preliminary evaluation of three types of filters was performed to determine if any of these materials met all of the above requirements. The filters tested were: a 90-mm diameter Solvinert filter made by Millipore Corporation with a 0.25 μm pore size, a 110-mm diameter high efficiency glass fiber filter made by Gelman, and a 47-mm Nuclepore filter made by General Electric Corporation with a pore size of 0.4 μm in diameter. All three of these filters meet the corrosive gas and temperature stated above. The weight stability of the Solvinert and glass fiber filters

were tested to determine the amount of sample which must be collected to obtain 3σ accuracy in the sample weight. Fifteen of the 90-mm Solvinert filters were dried in an oven for two hours at 135°C and then each weighed twice. The arithmetic mean of the weight deviations and the standard deviation in the mean was calculated. For a confidence level of 99%, the weight deviation was 0.201% or approximately 0.6 mg, since the filters has a tare weight of approximately 300 mg. Therefore, to obtain a 3σ accuracy of 1% using these filters, a sample of 60 mg must be collected. Glass fiber filters are very fragile and can lose considerable weight during sampling and subsequent filter handling. Three of the Gelman filters were loaded into a filter holder ten times each and weighed to determine the amount of weight loss due to the assembly procedure. The weight loss at a 99% confidence level was 0.126% or about 1 mg for a 800 mg tare weight filter. Using these filters, approximately 100 mg of sample must be collected to obtain the 1% accuracy. Greater weight loss can be expected during the actual use of these filters due to blow-off of glass fibers during sampling and water moisture variations.

The pressure drop characteristic of the Solvinert and the Nuclepore filters were tested in holders having stainless steel screen supports and Teflon back-up filters. The Teflon filters decreased the pressure drop by reducing the area restriction of the stainless steel screen. The 0.25 μm Solvinert filter was tested in a filter holder having an area of 0.06 in^2, while a 1.5 in^2 filter holder was used to test the 0.4 μm Nuclepore filters. The pressure drop curves determined for these two filters are shown in Figure 29. By using the manufacturer's information, it was possible to extrapolate this data to filters of different sizes and pore diameters.

Besides having a lower pressure drop, the Nuclepore filters have two other advantages over the Solvinert filter: low tare weight and greater strength. The Nuclepore 47-mm filter weighed only 20 mg. The Solvinert filters are very brittle and were difficult to handle during the field test at TVA. We do not expect there will be a weight stability problem with the Nuclepore filters because of their low tare weight. The Pallflex Products Corporation's Ultipore 0.35 filter may also be usable. The manufacturer's data shows that the pressure drop-flow rate curve for a 47-mm filter is the same as for the 0.5 μm-90 mm Solvinert filter. The weight stability for this filter and the Nuclepore filter need to be evaluated.

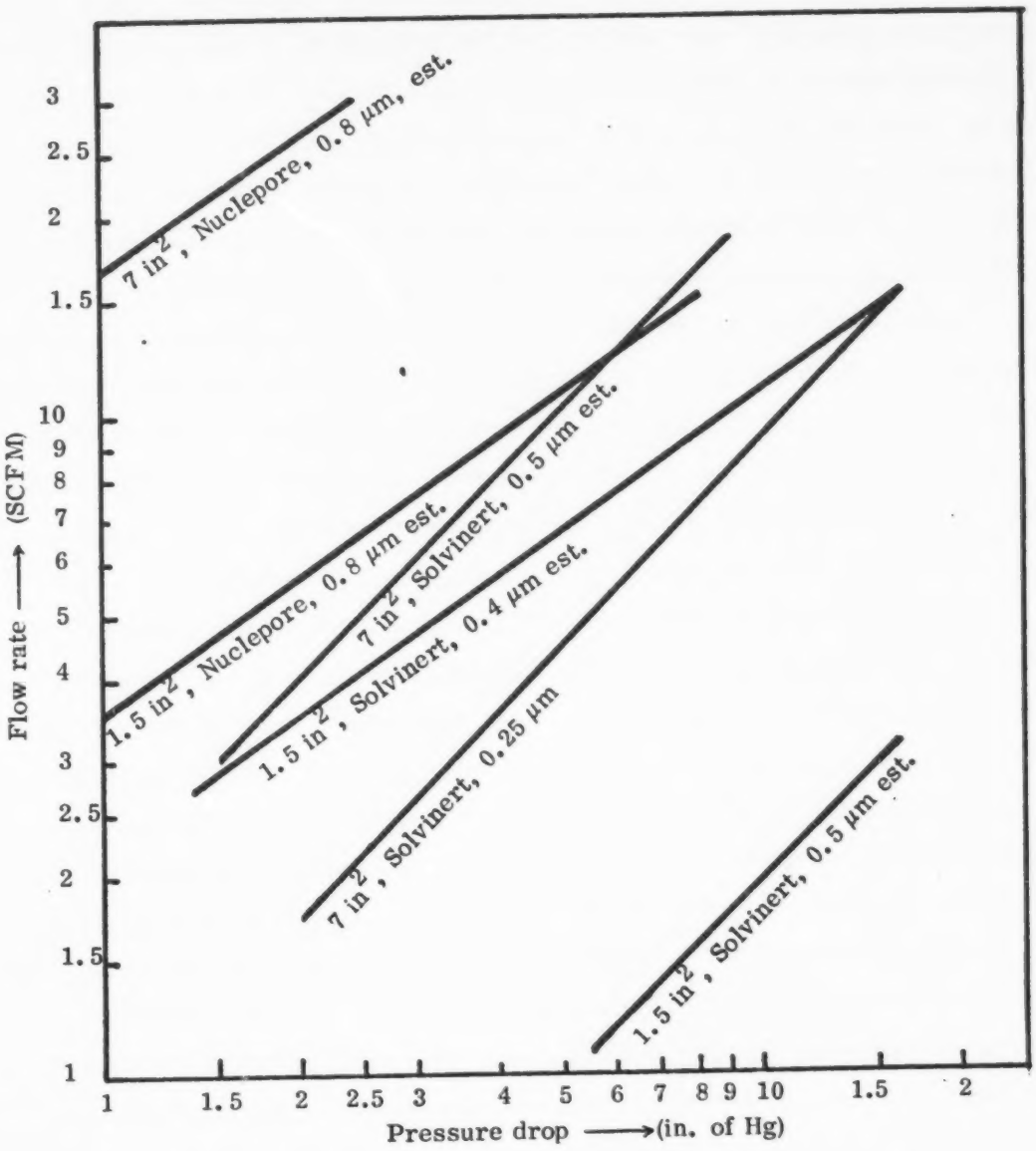

FIGURE 29 Pressure drop vs. flow rate for several filters in typical filter holders with teflon backup filter to reduce the pressure drop.

III. Summary of Phase II

An automatic particle monitor is attractive mainly because manual collection and analysis of four particulate samples in eight hours from six gas stream is difficult and costly as it introduces high manpower requirements and a great possibility of missed or improperly treated samples. An automatic monitor would provide, or at least approach, continuous monitoring, more timely data, and additional information about the particles such as their iron, sulfur and magnesium content.

A conceptual design for an automatic particle monitor system which is technically and economically feasible has been developed and reported previously.[25] The monitor will sample six points simultaneously using a cascaded cyclone and slot impactor to size-selectively collect the sample; a β-ray mass gauge and an x-ray fluorescence spectrometer to analyze the mass and composition of the particle-size fractions collected; and a computer to control the monitors as well as collect and analyze the data. Six particle-collection and -analysis subsystems will be controlled by two computers. At the inlet of each of the three scrubbers, one particle size fraction will be collected and analyzed each minute while only one analysis every two to three minutes will be feasible at the outlet of the scrubber. The β-ray mass gauges will require 10-30 sec counting times for each size fraction analyzed. After mass analysis, the particles will be moved to the x-ray fluorescence analyzer where an analysis of the elemental composition will be made after a 10-sec count. One of the major functions in data reduction will be the elimination of interferences in the x-ray fluorescence spectrometer due to particle-size and matrix-composition variations; this will be accomplished by physical and/or mathematical methods.

The major advantage of the design is the use of proven techniques. β-ray absorption and x-ray fluorescence are well understood phenomena and have been used in many process control applications. Particle sampling and collection using cyclones and impactors are being thoroughly investigated under the same contract for which the automatic monitor is being developed. The integration of these techniques with computer control is certainly feasible.

The maximum cost for constructing and maintaining the automatic monitor is estimated to be $358,710. The estimated cost for manual sampling includes the development program for the manual methods and the equipment and manpower required for sampling during 30 weeks of scrubber tests but excludes the cost of analyzing the collected samples and training the sampling personnel. This cost alone is $425,228. If the demonstration program lasts longer than 30 weeks and if the two cost items excluded are added, the total cost for using the manual method will be much greater. Based on the figures described, the automatic monitor is economically feasible (see Table 19).

From the cost data for the automatic monitor, several conclusions about cost reductions have been made. The large number of duplicate components make searching the market for the least expensive components important. In addition, a design which eliminates a few components will be considerably cheaper; as is shown, a more efficient computer system which would reduce the number of components for that system is feasible. In this way, price reductions of $20,000 to $30,000 can be achieved without any sacrifice in instrument performance. By reducing instrument performance or the number of sampling points to be measured simultaneously, even larger reductions in hardware and development costs can be achieved.

Table 19 Cost Data Summary

Item	Cost Comparison	
	Manual method	Automatic method
Hardware, (including replacement parts)	$156,728	$173,768
Labor:		
Development Program	104,000	184,942 (includes repairs at TVA during demonstration program)
Sampling manpower (assuming 30 weeks demonstration program)	164,500	automatic
Cost of chemical analysis of collected samples	unknown	automatic
Total	$425,228	$358,710

References

1. Bechtel Corporation, Alkali scrubbing test facility, Phase I: preliminary engineering, report to NAPCA, NAPCA contract PH 22-68-67 (May, 1969).

2. Bechtel Corporation, Alkali scrubbing test facility, Phase II: Design engineering, design criteria, report to NAPCA, NAPCA contract PH 22-68-67 (May, 1970).

3. S. M. Blacker, Evaluation of the Andersen Stack Sampler, A report of field test, NAPCA, 1970.

4. Environmental Research Corporation: Report of results of Andersen Stack Sampler evaluation tests, Submitted to HEW, 1970.

5. Walter C. McCrone Associates, Inc., Particulate measurements for fossil-fuel combustion sources. A report to NAPCA on the state of the art, section 6, NAPCA contract CPA 22-69-130 (July, 1970).

6. Environmental Research Corporation, "Report of Results of Andersen Stack Sampler Evaluation Tests," December 2, 970.

7. Schemel, G. A., "The Density of Uranine Particles Produced by a Spinning Disc Aerosol Generator. "J. of Amer. Indust. Hygiene Assoc., September, October 491-492.

8. Wiland, Geisel, "Calculating the Particle Size Distribution of a Duct by Means of Fractional Separation Efficiency Curves and Total Efficiency Curves," Staub-Reinhart, Luft. 28, 25-28 (1968).

9. Hilbert Schenck, Theories of Engineering Experimentation, 50-53, McGraw-Hill Book Co., (1968).

10. Muschelknautz, E., and K. Brunner, "Experiments with Cyclones," Chem.-Ing.-Techn., 39, pp 531-538 (1967).

11. Rosin, P., and E. Rammler, Journal of Inst. of Fuel, 7, p. 29 (1933).

12. "Air Pollution Engineering Manual," PHS publication, 99-AD-40, U. S. Dept., HEW (1967).

13. N. W. First, "Fundamental Factors in the Design of Cyclone Dust Collectors," Sc. D. discertation, Harv. Univ. (1950).

14. W. Barth, "Calculation and Design of Cyclone Separators on Basis of Recent Investigations," etc.

15. Muschelknautz, E., and W. Krambrock, The aerodynamic coefficients of the cyclone separator as based on recent, improved measurement, Chem. Ing. Tech. 42, 247-255 (1970).

16. Muschelknautz, E., Design of cyclone separators in the engineering practice, Staub-Reinholdt Luft 30, 1-12 (1970).

17. Stairmand, C. J., The design and performance of cyclone separators, Trans. Inst. Chem. Engrs. 29, 356-383 (1951).

18. Lipman, M. and A. Kydonieus, A multistage aerosol sampler for extended sampling intervals, Am. Ind. Hyg. Assoc. J., 730-7 (1970).

19. Freudenthal, P., High collection efficiency of the Aerotec-3 cyclone for submicron particles, Atmos. Environ. 5, 151-4 (1971).

20. Cochman, J. C., and H. M. Moseley, Simplified method for determining cascade impactor stage efficiencies, Am. Ind. Hyg. Assoc. J., 62-67 (1967).

21. Walter C. McCrone Associates, Inc., Particulate measurements for fossil-fuel combustion sources. A report to NAPCA on the state of the art, sections 3, 4 and 5 NAPCA contract CAP 22-69-130 (July, 1970).

22. G. A. Sehmel, Particle sampling bias introduced by Anisokinetic Sampling and deposition within the sampling line, American Industrial Hygiene Association Journal, Nov-Dec., 1970.

23. Personal communication with Meryl Jackson, Freeman Laboratory, Chicago.

24. W. Strauss, Industrial Gas Cleaning, Pergamon Press Ltd., First Edition, 1966.

25. N. A. Fuchs, The Mechanics of Aerosols, Pergamon Press, Ltd., 1964.

26. S. Badzioch, Correction for Anisokinetic Sampling of Gas-borne Dust Particles, Journal of the Institute of Fuel, March, 1960.